AD-A086 875 PRINCETON UNIV NJ DEPT OF MECHANICAL AND AEROSPACE --ETC F/G 20/4
EXPERIMENTAL STUDY OF THREE-DIMENSIONAL SHOCK WAVE TURBULENT BO--ETC(U)
JUL 80 D S DOLLING, S M BOGDONOFF N60921-78-C-006A
UNCLASSIFIED MAE-1483 NL

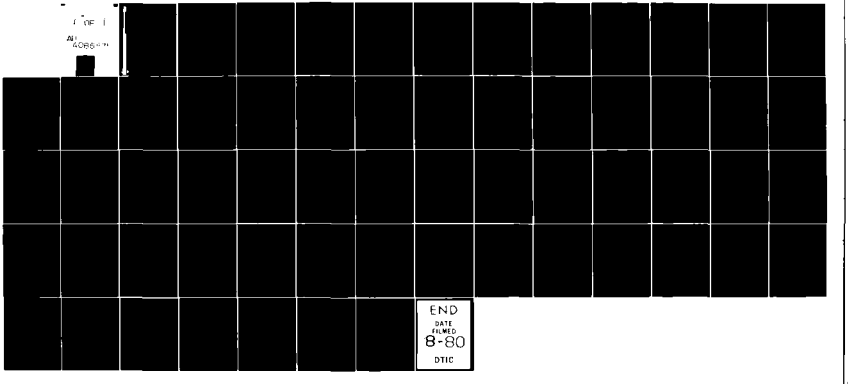

REPORT MAE-1483

LEVEL II

(12)

EXPERIMENTAL STUDY OF THREE-DIMENSIONAL SHOCK WAVE TURBULENT BOUNDARY LAYER INTERACTION - SCALING OF SHARP AND BLUNT FIN-INDUCED FLOWFIELDS

DAVID S. DOLLING
SEYMOUR M. BOGDONOFF

PRINCETON UNIVERSITY
DEPARTMENT OF MECHANICAL AND AEROSPACE ENGINEERING
GAS DYNAMICS LABORATORY, FORRESTAL CAMPUS
PRINCETON, NEW JERSEY

JULY 1980

FINAL REPORT FOR PERIOD 4 MAY 1978 - 3 MAY 1980

APPROVED FOR PUBLIC RELEASE; DISTRIBUTION UNLIMITED

PREPARED FOR:

NAVAL SURFACE WEAPONS CENTER
WHITE OAK LABORATORY
SILVER SPRING, MD

NAVAL AIR SYSTEMS COMMAND
DEPARTMENT OF THE NAVY
WASHINGTON, D.C.

UNCLASSIFIED

SECURITY CLASSIFICATION OF THIS PAGE (When Data Entered)

REPORT DOCUMENTATION PAGE	READ INSTRUCTIONS BEFORE COMPLETING FORM
1. REPORT NUMBER: MAE-1483	2. GOVT ACCESSION NO.: AD-A086 875
3. RECIPIENT'S CATALOG NUMBER	
4. TITLE (and Subtitle): Experimental Study of Three-Dimensional Shock Wave Turbulent Boundary Layer Interaction - Scaling of Sharp and Blunt Fin-Induced Flowfields	5. TYPE OF REPORT & PERIOD COVERED: Final Report, May 4, 1978 - May 3, 1980
	6. PERFORMING ORG. REPORT NUMBER
7. AUTHOR(s): D. S. Dolling, S. M. Bogdonoff	8. CONTRACT OR GRANT NUMBER(s): N60921-78-C-0068
9. PERFORMING ORGANIZATION NAME AND ADDRESS: Princeton University, Gas Dynamics Laboratory, Forrestal Campus, Princeton, NJ 08544	10. PROGRAM ELEMENT, PROJECT, TASK AREA & WORK UNIT NUMBERS: 61153N; O; WR02-302-003;O
11. CONTROLLING OFFICE NAME AND ADDRESS: Naval Surface Weapons Center, White Oak, Silver Spring, MD 20910	12. REPORT DATE: July 1980
	13. NUMBER OF PAGES: 58
14. MONITORING AGENCY NAME & ADDRESS (if different from Controlling Office): Naval Air Systems Command, Department of the Navy, Washington, D. C. 20361	15. SECURITY CLASS. (of this report): Unclassified
	15a. DECLASSIFICATION DOWNGRADING SCHEDULE

16. DISTRIBUTION STATEMENT (of this Report)

Approved for public release; distribution unlimited

17. DISTRIBUTION STATEMENT (of the abstract entered in Block 20, if different from Report)

18. SUPPLEMENTARY NOTES

19. KEY WORDS (Continue on reverse side if necessary and identify by block number)

Three-dimensional shock wave-boundary layer interaction
Blunted fin-induced interaction
Turbulent boundary layer

20. ABSTRACT (Continue on reverse side if necessary and identify by block number)

An experimental study of three-dimensional (3-D) shock wave turbulent boundary layer interaction has been carried out. Interactions generated by fin models having sharp and hemi-cylindrically blunted leading edges have been studied. Tests have been made using incoming turbulent boundary layer varying in thickness in the ratio of about 4:1. Extensive surface property measurements have been made on the test surface on which the incoming boundary layer developed and on the fin itself. All of these tests were carried out at a nominal

DD FORM 1 JAN 73 1473 EDITION OF 1 NOV 65 IS OBSOLETE

UNCLASSIFIED

SECURITY CLASSIFICATION OF THIS PAGE (When Data Entered)

freestream Mach number of 3, a freestream unit Reynolds number of about 63 million per meter, and under approximately adiabatic wall conditions.

The emphasis in the study reported on in this paper was on two main areas. First, to determine the key geometric and/or flow parameters controlling the overall scaling and characteristics of both blunt and sharp fin-induced interactions. Second, to identify the conditions under which both blunt and sharp fins induce interactions have the same local scale and characteristics.

SUMMARY

An experimental study of three-dimensional (3-D) shock wave turbulent boundary layer interaction has been carried out. Interactions generated by fin models having sharp and hemi-cylindrically blunted leading edges have been studied. Tests have been made using incoming turbulent boundary layers varying in thickness in the ratio of about 4:1. Extensive surface property measurements have been made on the test surface on which the incoming boundary layer developed and on the fin itself. All of these tests were carried out at a nominal free-stream Mach number of 3, a freestream unit Reynolds number of about 63 million per meter, and under approximately adiabatic wall conditions.

The emphasis in the study reported on in this paper was on two main areas. First, to determine the key geometric and/or flow parameters controlling the overall scaling and characteristics of both blunt and sharp fin-induced interactions. Second, to identify the conditions under which both blunt and sharp fins induce interactions have the same local scale and characteristics.

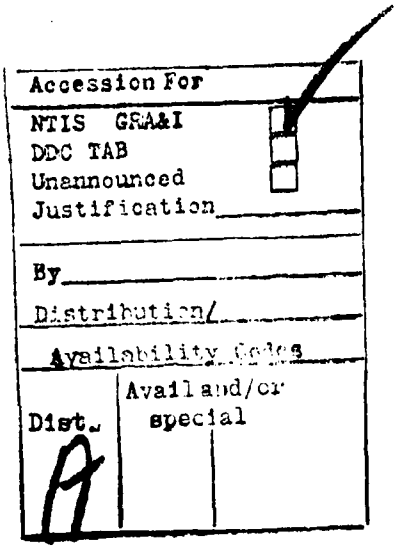

TABLE OF CONTENTS

LIST OF FIGURES

NOMENCLATURE

D	fin leading edge diameter = DIA
L_u	upstream influence as defined in Section 3.1
LSH	distance along shock wave, measured from leading edge
M	freestream Mach number
PST	undisturbed freestream static pressure
PW	wall static pressure
$\overline{P}$	PW/PST
X	coordinate parallel to the tunnel axis measured from the fin leading edge
XS	distance along instrumentation line measured from the undisturbed freestream shock wave position
Y	coordinate normal to the X axis in the plane of the test surface measured from the fin leading edge
α_F	fin angle of attack
β_{SH}	shock wave angle
δ	local undisturbed boundary layer thickness just ahead of the interaction pressure rise = DELTA
δ_o	undisturbed boundary layer thickness at fin leading edge

1. INTRODUCTION

Under the sponsorship of Naval Air Systems Command, and other agencies, the Gas Dynamics Laboratory of Princeton University has been carrying out experimental studies of three-dimensional (3-D) shock wave turbulent boundary layer interactions. These interactions are typical of those which can occur at wing/fuselage or fin/body junctions on supersonic aircraft or missiles and in many types of engine inlets. Despite their practical significance, both in these specific cases, and in the most general sense, few experimental studies have been sufficiently wide ranging and detailed enough to gain any fundamental understanding of the controlling parameters of these flowfields.

In the earliest program carried out at the Gas Dynamics Laboratory, surface property distributions and detailed flowfield surveys were obtained in an interaction generated by a skewed shock wave. The shock was generated by a sharp leading edged fin model mounted normal to a flat surface (Fig. 1) on which a high Reynolds number, Mach 3, turbulent boundary layer developed. Full details of this investigation, carried out by Oskam, et al, are given in Refs. 1 through 5. Oskam's measurements, now being used as a baseline for comparison with numerical computer codes, were instrumental in clearly showing that some of the early ideas of the flowfield structure were incorrect.

The investigation of the skewed shock interaction answered several controversial questions, but also posed many new and puzzling problems. These included the fundamental question of how the interaction, which had been studied at some distance from the shock generator, would be influenced by the details of the fin leading edge geometry. To examine this, a detailed experimental program, using hemi-cylindrically blunted fins , was carried out under the sponsorship of Naval Air Systems Command. Detailed surface property distributions

were measured over a wide range of fin leading edge diameters and angles of attack for two different incoming turbulent boundary layers. Details of this test program and some of the early results are given in Refs. 6 through 10. The data generated in this first experimental study has been compiled in tabular and graphical form and is available as Ref. 11.

In the first phase of the study reported on here, an examination was made of the experimental data base generated in the earlier investigation. The main objective was to identify the key geometric and/or flow parameters which determine the scale and characteristics of the interaction flowfield. The effects of incoming boundary layer characteristics and variable shock wave strength have been examined, and techniques have been developed for scaling the interaction length in the streamwise, lateral, and vertical directions. This is a complex problem since geometric and/or flow parameters which are of importance in one region of the flowfield may be relatively unimportant in others. In addition, different regions of the flowfield gradually merge and in these regions more than one parameter may be significant. Particular attention in this investigation has been focussed on determining under what conditions the blunt fin induced interaction flowfield takes on the character and scale of the sharp leading edged fin case. Where possible, experimental data from other investigators has been used for comparison and for assistance in identifying dominant parameters and trends.

To assist in this analysis, supporting experiments have been made in critical areas of a broad test matrix. These have included detailed surface pressure distributions along the plane of symmetry ahead of blunt fins and along streamwise rows out to a lateral distance (Y) of four leading edge diameters (D). Two incoming boundary layers were used, having thicknesses in the ratio of 4:1. In all of the blunt fin studies, the freestream shock wave shapes were determined

experimentally. For consistency and accuracy in comparisons of the earlier sharp leading edged fin data with those of the blunt fin, experiments were also carried out to measure the shock wave angles generated by the sharp leading edged model. An accurate knowledge of the shock wave location in the free-stream flowfield is essential since this case serves as a baseline for the blunt fin study.

All of the measurements carried out in the test matrix above were made on the surface on which the incoming boundary layer developed. They did not provide any information on the interaction's characteristics and scaling in the vertical direction. To examine this, a blunt fin instrumented with pressure tappings was constructed and tested in four different incoming turbulent boundary layers. This fin, and others of different diameter, but uninstrumented, were also used in a study sponsored by the Army Research Office, in which the role of the ratio D/δ was examined. This is described in Ref. 12. From these two studies, fin leading edge and body pressure distributions for the instrumented model are available for incoming turbulent boundary layers ranging in thickness from .127 cm (0.050") to 2.03 cm (0.8"). A detailed presentation of this data and discussion of the vertical scaling of the blunt fin-induced interaction has been given in Refs. 9, 10 and 12 and will not be repeated in this report.

In the blunt fin study, schlieren and shadow photographs have shown that the shock wave structure ahead of and around the fin leading edge is highly unsteady. Such unsteadiness has important implications, since it is not clear that any mean or averaged flowfield structure, as is frequently sketched in the literature, has any physical significance. This unsteadiness will be investigated as part of a future program under the joint sponsorship of Naval Air Systems Command and the Army Research Office.

2. EXPERIMENTAL PROGRAM

2.1 Wind Tunnel Facility

The experiments were carried out in Princeton University's 20 cm. x 20 cm. (8" x 8") high Reynolds number, supersonic, blowdown tunnel. This facility uses high pressure air stored at atmospheric temperature and can be operated at stagnation pressures in the range 4×10^5 to 3.4×10^6 Nm^{-2} (60-500 psia). The nominal freestream Mach number is 3.

All the tests reported on here were made at a stagnation pressure of 6.8×10^5 Nm^{-2} (100 psia) giving a freestream unit Reynolds number of approximately 6.3×10^7 m^{-1} (1.6×10^6 in^{-1}). The models were at near adiabatic wall temperature for all tests.

2.2 Test Models and Instrumentation

Two basic configurations were used. They are shown in Fig. 2. The model 1 configuration used the tunnel floor boundary layer. This is a 2-D, fully turbulent, equilibrium boundary layer which has been surveyed in detail along the entire test section, Ref. 13. At the test station, the incoming boundary layer was 1.27 cm (0.5") thick.

Model 2 used the boundary layer which developed on a horizontal, sharp leading edged flat plate which spanned the tunnel. In this case, the boundary layer thickness at the test station was about 0.33 cm (0.13").

The tunnel floor of the model 1 study and the flat plate of model 2 were both instrumented with rows of pressure tappings parallel to the X axis (Fig. 3). The fin models could be translated laterally and longitudinally relative to these fixed rows such that highly detailed pressure distributions could be obtained.

A total of ten different fins have been tested. These include the sharp leading edged model and blunt fins having leading edge diameters D in the range 0.1 cm $\leq$ D $\leq$ 2.54 cm. Pressure distributions were measured over the range $0 \leq Y/D \leq 110$ at angles of attack between 0^{o} and 12^{o}. The coordinate system used to present the data is shown in Fig. 3. The coordinate X_s is measured relative to the undisturbed freestream shock wave location.

2.3 Shock Wave Shape Determination

For data analysis purposes it is essential that the freestream shock wave location is known accurately. In an earlier study, Ref. 6, shock wave shapes had been experimentally determined from shadowgraphs for all of the blunt leading edges over the angle of attack range $0 \leq \alpha_F < 12^{o}$. For the sharp leading edged fin, shock wave locations were calculated from the oblique shock relations, knowing the freestream Mach number and fin geometric angle of attack.

However, inviscid calculations ignore the boundary layer displacement thickness effect which causes an additional flow deflection and thus increases the shock wave angle. The increment in angle is typically small, but at large lateral distances away from the fin, small angle changes can lead to appreciable errors in determining the freestream shock wave location. To avoid such errors, and to provide consistency with the blunt fin measurements, shock wave angles were experimentally determined for the sharp leading edged fin. Figure 4 shows the measured shock wave angles compared to those determined theoretically.

3. DISCUSSION OF EXPERIMENTAL RESULTS

3.1 Introduction

The objective of the analysis of the experimental data was to determine the geometric and/or flow parameters controlling the scaling and characteristics of these 3-D interactions. The measurements have shown that different regions of the flowfield depend on different individual parameters or combinations of parameters. These different regions gradually merge and in no region is it possible to state categorically that only one parameter or another uniquely controls the scaling. However, the data base created in this experimental program has been wide-ranging enough to reach some conclusions concerning the relative importance of certain parameters in different regions of the flowfield and, in some cases, to define the approximate boundaries of these regions.

The discussion in this section is concerned with two main characteristics of the flowfield. First, the effect of flow and geometric parameters on upstream influence has been examined. In this context, upstream influence L_u is defined as the distance in the X direction from the undisturbed freestream shock wave to the initial rise in the surface pressure. Analytically, L_u can be accurately determined since the location at which the pressure P_w has risen a given amount (say, 1%) above the upstream undisturbed level (P_{ST}) can be easily calculated. Experimentally, pressure tappings have a finite spacing and difficulties may arise in accurately determining where $P_w/P_{ST} = 1.01$. Here, the experimental technique used to determine L_u is shown in the inset in Fig. 5. This method, compared to the analytic approach, will in general result in a lower value of L_u.

Second, entire interaction pressure distributions have been examined to determine under what conditions the scaling and characteristics of blunt and

sharp leading edged fin cases are approximately the same. This is a complex problem, since a number of different parameters are involved, but it is of practical importance, since it is then possible to determine the region of influence of the fin leading edge. This problem is addressed in Section 3.5.

3.2 Sharp Leading Edge Fin Studies

3.2.1 Princeton University Experiments

Upstream influence data from the model 1 and model 2 configurations are shown in Fig. 5. The data for each model are grouped around four values of Y. Each group corresponds to measurements along one row of pressure tappings for several angles of attack. Since the fin center of rotation was behind the leading edge, the value or Y for a given row of pressure taps increased with angle of attack. Over the range $0 \leq \alpha_F \leq 12°$, the increment in Y was 0.48 cm. Thus, as shown in the figure, the larger values of Y correspond to the higher angles of attack.

The plot indicates that there is a systematic decrease in L_u with increasing α_F. The trend is stronger for the thicker boundary layer data. This result was also noted by Oskam, Ref. 5. However, such an observation depends critically on the plotting coordinates. By a suitable choice of axes, the dependence of L_u on α_F can be eliminated. A closer look at the geometry of the experiment and how it changes with increasing α_F reveals the following. As α_F increases, the shock wave angle increases, and the location at which it crosses a fixed row of pressure tappings moves upstream. This is illustrated in Fig. 6. The figure shows that although the distance Y of the intersection point increases with α_F, both its distance from the fin body Y_F and the distance from the leading edge along the shock wave LSH, decrease. If L_u is replotted versus Y_F (Fig. 7a) or LSH (as in Fig. 7b), the trend with angle

of attack, shown in Fig. 5, is eliminated. This shows that, with a given boundary layer, upstream influence depends only on the distance along the shock wave (or distance away from the fin) and not on the interaction pressure rise.

Although the effect of the shock wave pressure ratio has been eliminated, the influence of boundary layer thickness remains. Since $L_u = 0$ at LSH (or Y_F) = 0 , the curves approach one another in the region of the origin, and here, there is an approximate independence of boundary layer thickness. Figure 8 shows pressure distributions from the model 1 and 2 studies which illustrate this. This result is obviously specific to this set of tests. Use of thicker (or thinner) boundary layers would change the location at which the characteristics of the interaction could be considered as being approximately independent of δ .

Oskam, Ref. 5, attempted to correlate the upstream influence from the model 1 and 2 studies, but was not successful. Figure 9 shows the result. In Oskam's notation δ is the local boundary layer thickness at the start of the pressure rise, and δ_{AVE} is the average value of δ between the leading edge and the given value of Y . In this form, the angle of attack effect is still present, and the two data sets do not even approximate a single curve. However, using a similar technique, but in this case non-dimensionalizing both L_u and LSH by δ , an approximate correlation of the two data sets can be obtained. The result, shown in Fig. 10, strongly suggests that the incoming boundary layer characteristics do effect the interaction scale.

Based on what is known about the physical flowfield structure, it is unlikely that the extent of upstream influence can be accurately correlated using a single parameter such as δ . At a given Y , ahead of the initial pressure rise, there is a known incoming 2-D (in the mean sense) turbulent, boundary layer. Downstream of the pressure rise, coming from stations closer

to the fin, is a crossflow moving approximately along the shock wave direction. This crossflow consists of the low momentum boundary layer fluid which is unable to negotiate the streamwise pressure gradient and is consequently swept outwards. This crossflow interacts with the incoming boundary layer, which, in turn, adds to it. Simply using δ to scale L_u ignores this, so that although δ would appear important to the scaling process, it may be some function of δ, rather than δ alone. A similar problem exists in using δ to scale LSH. However, the fact that this simplistic approach does result in an approximate correlation does indicate that there is a dependency of the upstream influence on a parameter of the incoming boundary layer.

This in turn raises the more fundamental question of which parameter of the boundary layer is more physically appropriate. From the simplest point of view, L_u would depend on both the characteristics of the incoming layer and the amount of crossflow. The latter will depend on the details of the incoming profile, particularly those close to the wall, where the lowest velocities and largest momentum deficit occur. For the two model configurations tested here, the ratios of δ/δ^* and δ/θ are approximately the same, such that replotting Fig. 10 with the axes scaled by δ^* or θ simply changes the numbers along those axes without altering the shape of the curve. Again, the same problem concerning the use of local or averaged values, as outlined in the paragraph above, also occurs here.

3.2.2 Other Investigations

To see if similar trends existed over a wider range of flow conditions, data from the studies of Law[14], Lowrie[15], McCabe[16], Peake[17] and Stanbrook[18] have been examined. All of these studies used the same model geometry as the Princeton study. The data span the range $1.6 \leq M_\infty \leq 5.9$, $0.24 \text{ cm} \leq \delta \leq .58 \text{ cm}$.

Several difficulties arose in evaluating these data sets and in extracting accurate values of L_u , δ and Y . In some cases, the spacing of streamwise pressure tappings resulted in inadequate resolution of the pressure distribution which can result in significant errors in L_u . In general, there is a lack of detailed information on the incoming boundary layer characteristics. Estimates of δ have been obtained primarily by interpolation but, in some cases by extrapolation. The freestream shock wave angles β_{SH} , necessary for determining the position $X_s = 0$, have been obtained from oblique shock wave theory. In none of these cases were they determined experimentally. The change in β_{SH} is typically small, but at small angles of attack and/or high Mach numbers, it can lead to significant errors in locating $X_s = 0$, particularly at large values of Y . However, despite the inevitable inaccuracies in the estimates of L_u , Y , δ, etc., some general trends can be observed.

The data of Law, at M = 5.9, plotted in the form L_u vs. Y are shown in Fig. 11. The data points shown span the range $6° \leq \alpha_F \leq 16°$ for two incoming turbulent boundary layers. Measurements were also made at $\alpha_F = 20°$, but the instrumentation did not extend far enough to pick up the initial pressure rise. The value of α_F is shown next to each point. This figure shows that these measurements have the same trends as the Princeton data, when plotted in this form, namely: a) decreasing L_u with increasing α_F at a fixed value of Y , b) at a fixed α_F a general trend of increasing L_u with increasing Y . At a fixed α_F no differences can be detected between the growth rate of L_u with Y for the two different boundary layers. The difference in δ is small (about 20%) such that any systematic trends may have been masked by one or more of the possible inaccuracies discussed above.

Replotted in the form L_u vs. LSH , or L_u/δ vs. LSH/δ as in Fig. 12, the data collapse onto an approximate straight line passing through the origin.

As in the Princeton data, L_u is independent of the pressure ratio across the shock wave, which in this case varies from about 2.26 to 6.50.

The only other set of tests at the same Mach number as the Princeton study was that of McCabe (M = 2.94). The incoming boundary layer, with a thickness of about 0.6 cm, is in between the two values tested in the Princeton study. However, most of McCabe's measurements were made close to the fin body, providing little overlap with the Princeton data. Figure 13 shows the McCabe and Princeton data plotted in the form L_u vs. LSH . The McCabe data have more scatter than the Princeton data. This is due mainly to the difficulty of determining L_u from pressure plots having poor spatial resolution. In the small overlap region, around LSH = 6 cm , the McCabe data falls approximately between the model 1 and 2 Princeton data. Replotted in the form L_u/δ vs. LSH/δ as in Fig. 14, the data sets correlate reasonably well. McCabe's data were all non-dimensionalized by the same value of δ , irrespective of location in the flowfield. This is because only one value of δ was given by McCabe, namely that upstream of the interaction. Since the shock wave is swept, δ will in general increase with Y . Such an effect is included in the Princeton data but not in McCabe's. On this basis, the δ used to scale the McCabe data is most likely an underestimate. A value of δ which was about 10% higher would reduce the discrepancy between the McCabe and Princeton data.

For experiments in which the freestream Mach number was varied such as Stanbrook's (M = 1.6, 1.8, 2.0), McCabe's (1.96, 2.94), Lowrie's (2.5, 3.44) and Peake's (2,4) there is a common trend of increasing L_u with increasing M . For the data set as a whole, this can best be seen in Fig. 15, where all of the data are plotted in the form L_u/δ vs. LSH/δ .

The general trend, at least for LSH/δ > about 20, is that L_u/δ increases with increasing Mach number, although there is little difference between

Peake's $M = 4$ data and Law's $M = 5.9$ data. Close to the fin ($LSH/\delta <$ about 20) there is a reasonable correlation of the data. Over 120 data points are clustered in that region, but they only span the range $1.6 < M_\infty < 2.95$.

3.2.3 Concluding Remarks on Sharp Leading Edge Fin Studies

Measurements made in the Princeton study indicate that for a given incoming turbulent boundary layer, the upstream influence does not depend on the pressure ratio across the shock wave. It depends only on distance LSH along the shock wave, measured from the fin leading edge. Alternatively, as noted in the discussion, the same trends are observed with respect to Y_F, the distance from the shock wave to the fin surface.

Tests at the same freestream Mach number but with different incoming turbulent boundary layers show that at a given value of LSH, L_u is larger for the thicker boundary layer. An approximate correlation of these data sets can be obtained by non-dimensionalizing both LSH and L_u by δ, the local thickness of the incoming boundary layer. Other forms of scaling (i.e., by δ^* or θ) do not modify this result and there is a need for further work to determine which of these parameters (if any) is most appropriate and in what functional form it should be used. The most important aspect of this approximate correlation is in showing that the interaction scale depends on the properties of the incoming boundary layer.

Other experimental data exhibit similar trends to those observed in the Princeton study. Data at the same freestream Mach number but with a different incoming turbulent boundary layer can be correlated with the Princeton data using a simple scaling procedure. When plotted in the form L_u/δ vs. LSH/δ, the combined data sets indicate a trend of increasing L_u/δ with increasing Mach number. This trend becomes increasingly more pronounced with increasing distance outboard.

3.3 Blunt Fin Studies

Before presenting and discussing the experimental results, the effect of leading edge blunting on the freestream shock wave whape will be briefly described. An accurate knowledge of the shock wave's location in the flowfield is important since certain features of the interaction can be correlated on the basis of the local shock wave properties. In addition, the process whereby the blunt fin-induced interaction takes on similar characteristics to the sharp leading edged case is intimately connected to the local shock wave characteristics. For brevity, the sharp leading edged model will from now on be referred to as the s.l.e. fin.

3.3.1 Blunt Fin-Induced Shock Wave Shapes

The blunt leading edge causes a detached shock wave to form, whose shape, in the region close to the fin, is controlled by the leading edge diameter D. It was shown in the previous final report[6], that shock waves generated by different diameter fins could be represented by a single curve when plotted in the form X/D vs. Y/D. This plot showed that for $Y/D <$ about 10, the shock wave shape (and therefore its location in the flowfield) was virtually independent of the fin angle of attack (over the range 0° through 12°).

An alternative method of presenting the experimental results is to plot shock wave angle versus Y/D. This is done in Fig. 16 for two angles of attack, 0° and 12°. This format provides a means of easily comparing local shock angles at various α_F and, most importantly, allows direct comparison with the angles of oblique shock waves generated by s.l.e. fins at the same α_F.

It can be seen that the shock wave angle β_{SH} decreases rapidly with increasing Y/D. As noted earlier, for small values of Y/D (< about 10), β_{SH} is virtually independent of α_F. For $\alpha_F = 12°$, β_{SH} at Y/D of about 10 is only about 2° higher than the theoretical oblique shock wave angle (29.6°).

The same general behavior occurs at $\alpha_F = 0°$, but even at a Y/D of about 50, β_{SH} is still several degrees higher than the Mach wave angle. All other angles of attack behave in a similar way with the trend that the lower α_F , the greater the value of Y/D at which the blunted and s.l.e. shock wave angles differ by some small specified value.

3.3.2 Blunt Fin Experimental Results

In the earlier phases of this study[6-10], it was shown that the fin leading edge diameter was the appropriate parameter for correlating streamwise pressure distributions. At a fixed value of Y/D , the streamwise extent of the pressure distribution could be correlated by non-dimensionalizing X_S by D . Examples of the success of this approach were given in Refs. 7 and 9.

This correlation technique could be satisfactorily used independently of the thickness of the incoming turbulent boundary layer (at least over the range tested, 0.25 cm $\leq \delta \leq$ 2.03 cm). The extent of the region in which D was of primary importance and the significance (or otherwise) of δ and α_F was not clear at that time. This question will be addressed in this and the following sections. The approach adopted will be to examine the region close to the fin and then move progressively outboard in terms of Y/D (and Y/δ).

Centerline pressure distributions at zero angle of attack were shown in Ref. 9. The data spanned the ranges 0.25 cm $\leq \delta \leq$ 15.2 cm, 0.1 cm $\leq$ D $\leq$ 5.08 cm. The pressure distributions could be correlated using D as a streamwise distance scaling parameter, although it was noted that in terms of D , there was a weak, but systematic trend of decreasing upstream influence with increasing D/δ . This has been reported on in detail in Ref. 12. The conclusion from these data sets was that on the fin centerline the interaction scale depends, to first order, on D .

In the first Princeton study[6], measurements were made using eight different diameter fins. The lateral extent of the interactions generated spanned the range $2.5 \leq Y/D \leq 110$. The measurements showed that, close to the fin, a complex flowfield seemed to exist, in which multi-peaked streamwise pressure distributions and extremely large pressure gradients (lateral and streamwise) existed. Later studies[9,12] showed that this region was highly unsteady.

To examine this inner region in greater detail, pressure distributions were measured in the region bounded by $0 \leq Y/D \leq 4$. Two different diameter fins (D = 1.27 cm, 2.54 cm) were tested in both the model 1 and model 2 configurations (i.e., δ = 1.27 cm and 0.33 cm, respectively). All measurements were made at $\alpha_F = 0°$.

Upstream influence is shown plotted in Fig. 17. The dimensional plot, in the upper half of the figure has two important features. First, for a fixed diameter fin, increasing δ by a factor of 4 changes L_u only slightly. Second, for a fixed value of δ, the upstream influence depends primarily on D. Non-dimensionalizing both axes by D, as shown in the lower half of the figure, collapses the data onto a single line. This figure indicates that in the range $0 \leq Y/D \leq 4$, L_u depends primarily on D and is independent of δ, at least over the range tested. For future reference, it should be noted that the data shown in Fig. 17 span the range $0 \leq Y/\delta_o \leq 15$.

In this region, the interaction length and the characteristic features of the pressure distributions can also be correlated using D as a distance scaling parameter. Figure 18 shows pressure distributions at Y/D = 2. Plotted versus X_s, as in the upper half of the figure, the independence of the streamwise scale on δ and the direct dependence on D can be clearly seen. In terms of X_s/D, as in the lower half of the figure, the pressure distributions

correlate well. The pressure ratios at the two peaks are influenced by the ratio D/δ and this has been investigated in Ref. 12.

Figure 16 shows that at a given value of Y/D, within the range $0 \leq Y/D \leq \sim 6$, the local shock wave angle β_{SH} is fixed and independent of α_F. Since the correlation method outlined above applies at fixed values of Y/D, this strongly suggests that the local interaction structure depends critically on the local shock strength. It should be emphasized here that the complete interaction scale depends on the shock strength, although the upstream influence ahead of the shock wave does not. The validity of this argument will be demonstrated more forcefully later in this section. The reasons for the independence of the interaction extent on any obvious boundary layer scale are difficult to explain in a quantitatively satisfactory manner.

As noted earlier, in the first Princeton study, measurements were made in the range $2.3 \leq Y/D \leq 110$. The model 1 data spanned the range $2.3 \leq Y/D \leq 31.7$, and the model 2, $7.7 \leq Y/D \leq 110$, providing some overlap. At each value of Y/D, measurements were made at angles of attack 0° through 12°, in 2° increments.

A typical plot, in the form L_u/D versus Y/D for one fin ($D = 1.27$ cm) is shown in Fig. 19. Note that a dimensional plot would have identical trends since D is common to all the data points. Each of the four groups of points represents measurements along a given row of pressure taps at different angles of attack. As with the s.l.e. fin, larger values of Y (and Y/D) correspond to higher angles of attack.

For the two inner groups ($Y/D \sim 2$ and 4) L_u is, to within experimental accuracy, independent of α_F. At these values of Y/D, the shock wave location is fixed with the local angle being independent of α_F. Since Y/D for both sets increases slightly with increasing α_F, there is probably a

corresponding increase in L_u , but it is too small to accurately measure. The measured surface pressure distributions at $Y/D \sim 2$, from which these values of L_u were estimated, is shown in Fig. 20. It is clear that for all practical purposes L_u is constant. At $Y/D \sim 6$ and 8 , there is some variation (or scatter) of L_u with Y/D . At these latter two values of Y/D the shock wave angle plot shows that β_{SH} is close to the theoretical oblique shock value and, in addition, is no longer entirely independent of α_F . The significance of the latter will be discussed further in Section 3.5.

All of the upstream influence data from the model 1 and 2 studies, together with the data shown in Fig. 17 ($0 \leq Y/D \leq 4$), are shown in Fig. 21. A first look at the data plot suggests that scaling the axes by D is satisfactory out to Y/D of about 10 after which it breaks down. A closer look, however, shows up a number of anomolies, which disagree strongly with such a conclusion. For example, all the data measured along the inner row of pressure tappings in the model 2 study which span the range $7.7 \leq Y/D \leq 34$ correlate well with the model 1 data. However, data along the outer three rows of tappings in the model 2 study for the largest diameter fin tested ($D = .406$ cm), which are in the range $13.9 \leq Y/D \leq 29.1$, fall well below the model 1 data. In both cases the range of Y/D's is the same, yet one set of data correlate well with the model 1 data and the other does not.

Attempting to plot all of the data in this form poses a fundamental question concerning the physical nature of the flowfield. This question is how far away from the fin does using D as a scaling parameter make sound physical sense? This raises the additional question of whether at large distances from the blunt fin the resulting local interaction is the same as the local s.l.e. interaction? If so, then in these regions, it does not make any physical sense to use D as a scaling parameter, since it does not enter into the scaling of

the s.l.e. interaction. Before trying to clarify the anomolies mentioned above, the connection between the blunt and s.l.e. fin-induced interactions will be discussed.

3.3.3 Comparison of Interactions Induced by Blunt and Sharp Leading Edged Fins

The shock wave angle plot of Fig. 16 showed that within a few diameters of the fin centerline, β_{SH} is generally close to the theoretical oblique shock wave angle generated by a s.l.e. fin at the same angle of attack. The higher α_F, the shorter the distance Y/D in which this occurs.

For example, for $\alpha_F = 10°$ (or 12°), β_{SH} is almost constant for Y/D > $\sim$8. Based on this, an idea can be postulated, whose validity must be supported or refuted by the experimental evidence. At this α_F and for a given Y/δ, the interaction scale and the characteristics of the streamwise pressure distributions generated by different diameter blunt fins will be the same as that of a s.l.e. fin, providing all values of Y/D are greater than 8. Fixing α_F fixes the overall pressure rise whereas specifying Y/D > 8 ensures that all local values of β_{SH} are, to within a degree or two, the same as the theoretical oblique shock value (Fig. 16). The need for approximately fixing Y/δ will be discussed later. Under these conditions, the local interaction scale and characteristics will be independent of the nose blunting.

This idea hinges on the assumption that, for a given incoming boundary layer, the local interaction scale and characteristics depend on the local shock wave strength. In this region close to the fin the distinction must be made between β_{SH} and the overall pressure rise. The latter is fixed by the flow turning angle (i.e., fin angle of attack) whereas β_{SH} depends on the local value of Y/D. In the oblique shock case (or far from the blunt leading edge), specifying one of these parameters necessarily fixes the other. An example,

supporting this argument is shown in Fig. 22, where five pressure distributions from the model 2 study are plotted. They were generated by four different blunted fins and one s.l.e. fin and span the range $8.6 \leq Y/D \leq \infty$, ∞ corresponding to the s.l.e. case. Differences in detail exist, particularly around $X_S = 0$, but the interaction length scale and the general features are the same. In all five of these cases, at $\alpha_F = 10°$, and within the Y/D range specified, β_{SH} is the same to within 2 or 3 degrees.

A second example, from the model 1 study, spanning the range $5.8 \leq Y/D \leq \infty$ is shown in Fig. 23. In this example, the pressure distribution for $Y/D = 5.8$ has a different shape compared to the other cases. This supports the basic argument above since the shock wave angle plot (Fig. 16) shows that below Y/D of about 7, β_{SH} starts to increase rapidly.

Two important remarks must be made concerning the above result. First, the approximate boundary quoted above, namely Y/D of about 8, applies to an α_F of 10°. The shock wave angle plot of Fig. 16 shows that at lower values of α_F, larger values of Y/D are needed before β_{SH} from the blunt fin is close to that of the s.l.e. fin. Thus, for the <u>same</u> range of Y/D as Fig. 22, but at a <u>lower</u> α_F, this scaling of the entire interaction will break down. For example, the data sets at $\alpha_F = 10°$, which are plotted in Fig. 22, are shown at 4° in Fig. 24. The upstream influences are quite close, but there are radical differences in the streamwise scale and in the shape of the pressure distributions. In this case, the final pressure ratios are the same but the values of β_{SH} over the Y/D range vary considerably. As would be expected from the premise of the basic argument, the closest distribution to the s.l.e. model is the blunt fin having the largest value of D ($D = .10$ cm, $Y/D = 51$).

Second, at locations where all the distributions have the scale and characteristics of the s.l.e. case, then from that point outboard they will depend

on the same parameters as the s.l.e. case. This is illustrated in the following two figures, which will also be used to explain why in the above argument Y/δ must be fixed. Pressure distributions at $Y \sim 2.75$ cm ($Y/\delta = 2.2$) for a blunt fin ($D = .317$ cm) and an s.l.e. fin are shown in Fig. 25. The values of Y/D are 8.9 and ∞. The data correlate well, supporting the argument above. Further outboard, at $Y \sim 5.3$ cm ($Y/\delta \sim 4.2$), the data again correlate well, as shown in Fig. 26. In both the blunt and s.l.e. cases, the scale and characteristics of the interaction have changed in the same way with the same change in Y. In this region, the blunt fin-induced interaction develops in the same way as the s.l.e. fin, whose development depends on the boundary layer characteristics. Thus, although a change in Y neither changes the final pressure ratio or β_{SH}, it does change Y/δ which results in a change in the interaction scale.

Based on the above, it is possible to define a "nose-dominated" region of the flowfield. In this case, "nose-dominated" refers to a region in which the scaling and characteristics depend on the leading edge diameter. Outside of this region, the blunt and s.l.e. induced interactions have (at a given Y/δ and α_F) the same length scale and characteristics. In the example above, at $\alpha_F = 10°$, the approximate boundary between these two regions is at a Y/D of about 8. This boundary, in terms of Y/D, increases with decreasing α_F. In the limiting case of $\alpha_F = 0°$, the entire disturbed flowfield is effectively nose-dominated, since in the s.l.e. case there is no interaction at all. In practice, measurements at $\alpha_F = 0°$ from this study show that there is a significant disturbance (i.e., peak pressure ratio of 1.15) even at a Y/D of 110.

From the above, it is apparent that a nose-dominated region can be defined for specific values of D and α_F. This definition involves a similarity of the entire local interaction. In contrast, upstream influence, a physical length

scale, can be (and often is) the same for different interactions irrespective of whether the entire pressure distributions are the same. For example, both outside of the nose-dominated region (Fig. 22) and inside it (Fig. 24), L_u is approximately the same. The independence of upstream influence on both α_F and β_{SH} simplifies the problem to a certain extent, but at the same time there are further complicating issues.

The measurements indicate that outboard of Y/D of about 5 to 6, the upstream influences in the blunt and s.l.e. cases are approximately the same. Outboard of this value of Y/D , the blunt fin-induced upstream influence depends on the same parameters as the s.l.e. case. Increases in L_u/δ will depend on the increment in distance outboard $\Delta Y/\delta$ (or more accurately LSH/δ). Thus, a fixed increment ΔY outside of the region in which D dominates results in an increment in $\Delta Y/\delta$, the size of which depends on the local value of δ . In this region spanned by ΔY the scaling has a dependence on the boundary layer characteristics, and the details of the local interaction at the new value of Y will depend on the increment $\Delta Y/\delta$.

This is the case for the model 1 and 2 upstream influence data shown in Fig. 21, where a fixed increment in Y outside of Y/D of about 5 or 6, produces a different $\Delta Y/\delta$ in both cases. The outcome of this observation is that there are certain combinations of D , Y and δ such that scaling by D appears to produce a satisfactory correlation at large values of Y/D , as in Fig. 21. However, it is in a region where there is no solid physical argument for doing this. The data support the idea that outside of Y/D of about 5 or 6 the upstream influence acquires characteristics similar to the s.l.e. model and should be considered from this viewpoint. These conditions should be carefully distinguished from those at which the blunt and s.l.e. fins will

generate completely similar local interactions. The latter conditions are more complex, involving D , δ , Y , α_F and β_{SH} .

4. CONCLUDING REMARKS

An experimental study of 3-D shock wave turbulent boundary layer interaction has been carried out. Interactions generated by fins having sharp and hemi-cylindrically blunted leading edges have been studied. Tests were made with ten different fins over the angle of attack range $0 \leq \alpha_F \leq 12°$, using different incoming turbulent boundary layers. All of these tests were carried out at a nominal freestream Mach number of 3, a freestream unit Reynolds number of 63 million per meter, and under approximately adiabatic wall conditions. An analysis has been made of the surface property measurements made on the test surface on which the incoming turbulent boundary layer developed. This report presents elements of the analysis. Four of the more significant conclusions from this analysis are briefly outlined below.

a) For a given freestream Mach number and incoming turbulent boundary layer the upstream influence in a sharp fin-induced interaction is independent of the shock wave strength. At a fixed distance outboard of the fin, an increase in boundary layer thickness will result in an increase in upstream influence.

b) An approximate correlation between sets of upstream influence data from sharp fin-induced interactions measured at the same freestream Mach number but with different incoming turbulent boundary layers can be obtained using the local value of incoming boundary layer thickness as a distance scaling parameter. The correlation can be obtained in the form L_u/δ vs. LSH/δ (or Y_F/δ). This simple approach, although only approximate, indicates that the characteristics of the incoming boundary layer do affect the interaction scale. More work is needed to determine which of the boundary layer characteristics is physically appropriate, and in what functional form it should be used.

c) Measurements from this and other investigations indicate that in the range $0 \leq Y/D \leq \sim 5$, the interaction length scale and characteristics at a fixed fin angle of attack depend primarily on the leading edge diameter. In this region they are independent of the incoming turbulent boundary layer thickness.

d) Outboard of this inner region given in (c), the blunt fin interaction gradually acquires the length scale and characteristics of the sharp fin case. This occurs at a fixed value of Y/δ when the overall interaction pressure rise and local shock wave angle are in both cases about the same. The overall pressure rise depends on fin angle of attack, but the local shock wave angle depends on both angle of attack and Y/D. This means that the outboard location at which the scales are similar cannot be defined uniquely in terms of a number of leading edge diameters. It depends also on angle of attack. The higher the angle of attack, the closer inboard this location is.

5. REFERENCES

1. Oskam, B., Vas, I. E. and Bogdonoff, S. M., "An Exploratory Study of a Three-Dimensional Shock Wave Boundary Layer Interaction at Mach 3," Presented at the AGARD Symposium on "Flow Separation", May 1975, Report 1227.

2. Oskam, B., Bogdonoff, S. M. and Vas, I. E., "Study of Three-Dimensional Flow Fields Generated by the Interaction of a Skewed Shock Wave with a Turbulent Boundary Layer," AFFDL-TR-75-21, Final Report, February 1975. Also AMS Report 1264.

3. Oskam, B., Vas, I. E. and Bogdonoff, S. M., "Oblique Shock Wave/Turbulent Boundary Layer Interactions in Three Dimensions at Mach 3 - Part I," AFFDL-TR-76-48, Final Report, June 1976. Also AMS Report 1292.

4. Oskam, B., Vas, I. E. and Bogdonoff, S. M., "Mach 3 Oblique Shock Wave/ Turbulent Boundary Layer Interactions in Three Dimensions," AIAA Paper 76-336, July 1976.

5. Oskam, B., "Three-Dimensional Flow Fields Generated by the Interaction of a Swept Shock Wave with a Turbulent Boundary Layer," Princeton University Gas Dynamics Laboratory Report 1313. Also Ph.D. Thesis, Aerospace and Mechanical Sciences Department, Princeton University, December 1976.

6. Dolling, D. S., Cosad, C. D. and Bogdonoff, S. M., "Three-Dimensional Shock Wave Turbulent Boundary Layer Interactions - A Preliminary Analysis of Blunted Fin-Induced Flows," Report 1354, M.A.E. Department, Princeton University, October 1977.

7. Dolling, D. S., Cosad, C. D. and Bogdonoff, S. M., "Three-Dimensional Shock Wave Turbulent Boundary Layer Interactions - A Parametric Study of Blunt Fin-Induced Flows," AIAA Paper 78-159, January 1978.

8. Dolling, D. S., Cosad, C. D. and Bogdonoff, S. M., "Three-Dimensional Shock Wave Turbulent Boundary Layer Interactions - A Preliminary Analysis of Blunted Fin-Induced Flows," Boundary Layer Effects - Proceedings of the 7th U. S. Air Force/Federal Republic of Germany Data Exchange Agreement Meeting, AFFDL-TR-78-111, September 1978.

9. Dolling, D. S., Cosad, C. D. and Bogdonoff, S. M., "An Examination of Blunt Fin-Induced Shock Wave Turbulent Boundary Layer Interactions," AIAA Paper 79-0068, January 1979.

10. Dolling, D. S. and Bogdonoff, S. M., "Some Observations on the Anomolous Behavior of Fin-Induced Shock Wave Turbulent Boundary Layer Interactions," Proceedings of 4th U. S. Air Force/Federal Republic of Germany "Data Exchange Agreement Meeting - Viscous and Interacting Flow Field Effects," BMVg-FBWT 79-31, April 1979.

11. Dolling, D. S., "Three-Dimensional Shock Wave Turbulent Boundary Layer Interactions - Part I: Tabular and Graphical Presentation of Surface Pressure Distributions," Princeton University M.A.E. Report 1414, November 1978.

12. Dolling, D. S. and Bogdonoff, S. M., "Experimental Investigation of Three-Dimensional Shock Wave Turbulent Boundary Layer Interaction - An Exploratory Study of Blunt Fin-Induced Flows," Princeton University M.A.E. Report 1468.

13. Fernholz, H. H. and Finley, P. J., "A Critical Compilation of Compressible Turbulent Boundary Layer Data," AGARD-AG-223, June 1977.

14. Law, H. C., "Three-Dimensional Shock Wave Turbulent Boundary Layer Interactions at Mach 6," A.R.L. TR-75-0191, June 1975.

15. Lowrie, B. W., "Cross-Flows Produced by the Interaction of a Swept Shock Wave with a Turbulent Boundary Layer," Ph.D. Thesis, Cambridge University, 1965.

16. McCabe, A., "A Study of Three-Dimensional Interactions Between Shock Waves and Turbulent Boundary Layers," Ph.D. Thesis, University of Manchester, 1963.

17. Peake, D. J., "The Three-Dimensional Interaction of a Swept Shock Wave with a Turbulent Boundary Layer and the Effects of Air Injection on Separation," Ph.D. Thesis, Carleton University (Ottawa), 1975.

18. Stanbrook, A., "An Experimental Study of the Glancing Interaction Between a Shock Wave and a Turbulent Boundary Layer," ARC-CP-No. 555, 1961.

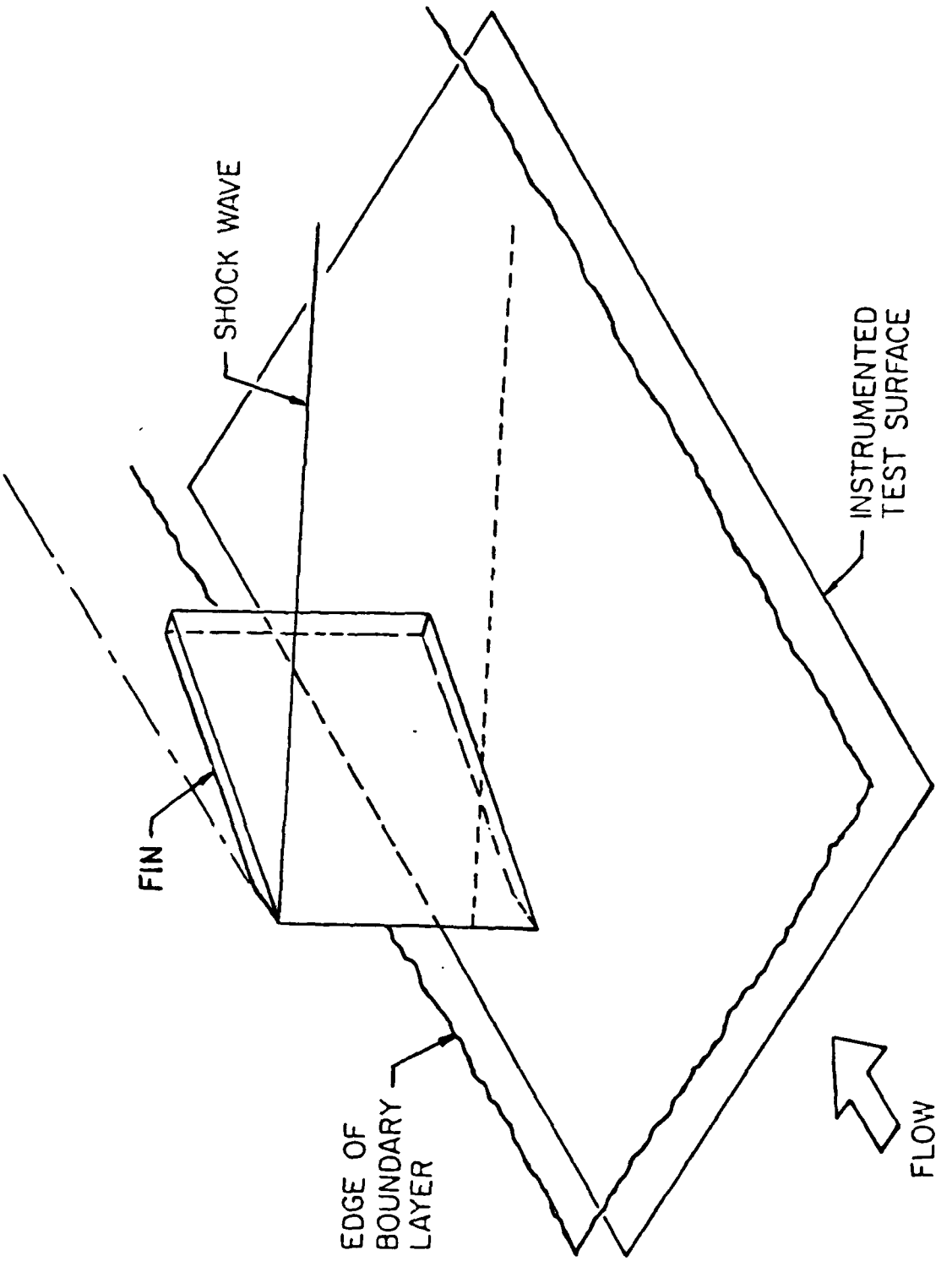

FIG. 1. Schematic of Basic Model Geometry

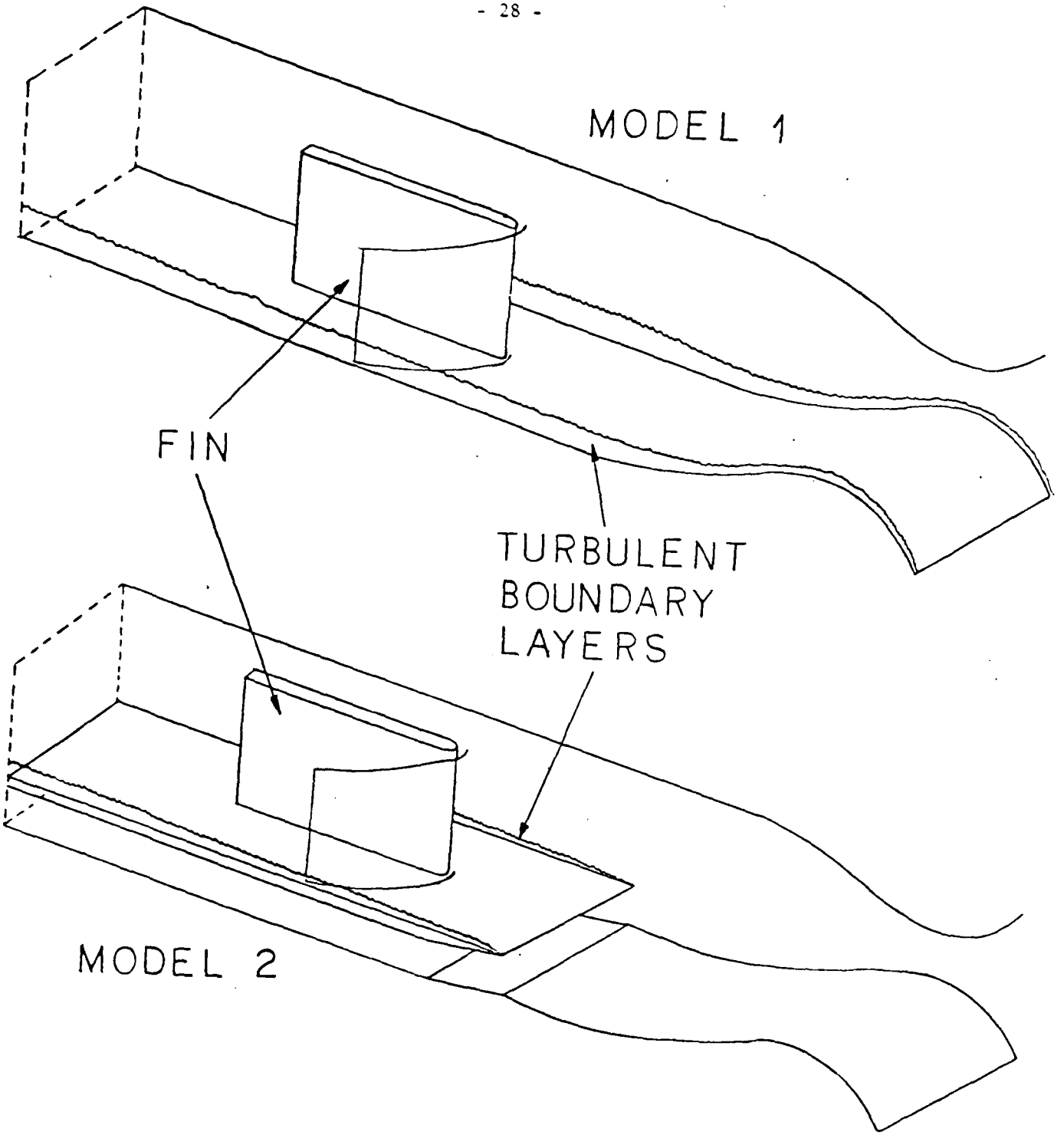

FIG. 2. Model 1 and 2 Configurations

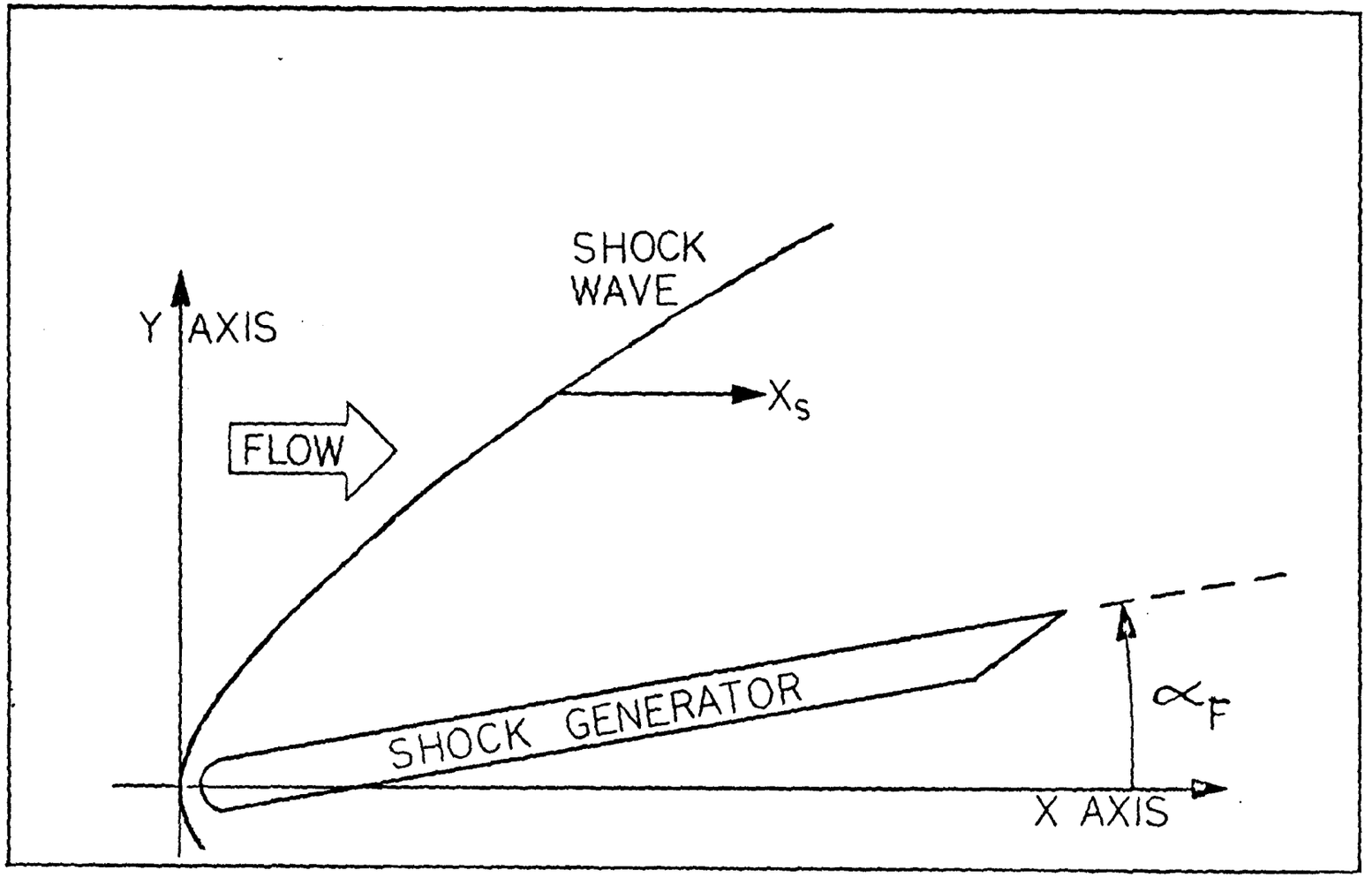

FIGURE 3. COORDINATE SYSTEM

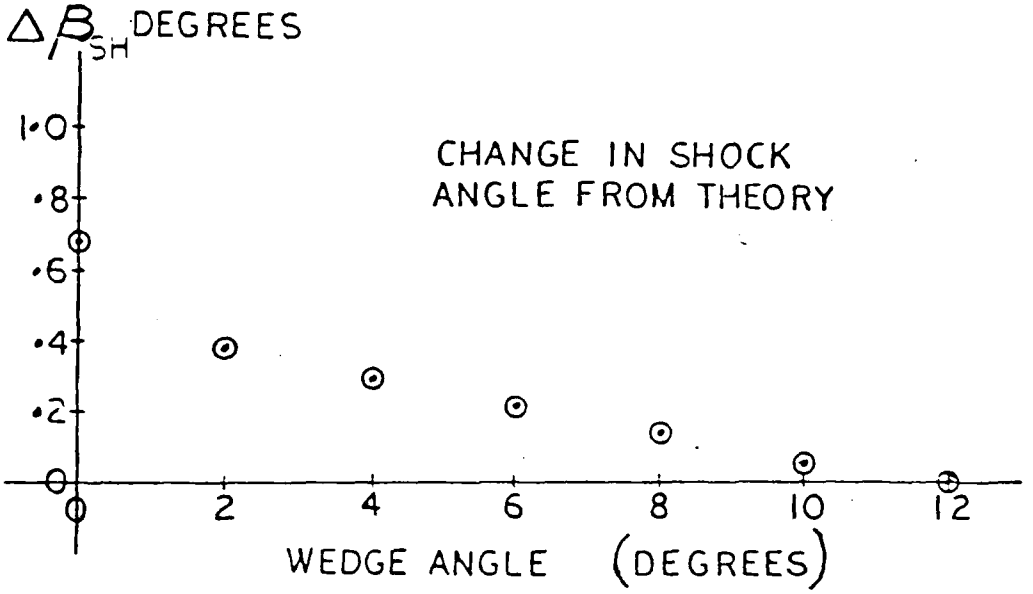

SUMMARY OF RESULTS

WEDGE ANGLE	SHOCK ANGLE THEORY	SHOCK ANGLE EXPER.	$\Delta\beta_{SH}$
0°	19·82	20·5	·68
2°	21·22	21·6	·38
4°	22·71	23·0	·29
6°	24·29	24·5	·21
8°	25·97	26·1	·13
10°	27·75	27·8	·05
12°	29·62	29·6	——

FIG. 4. Sharp Fin Shock Wave Angle Measurements

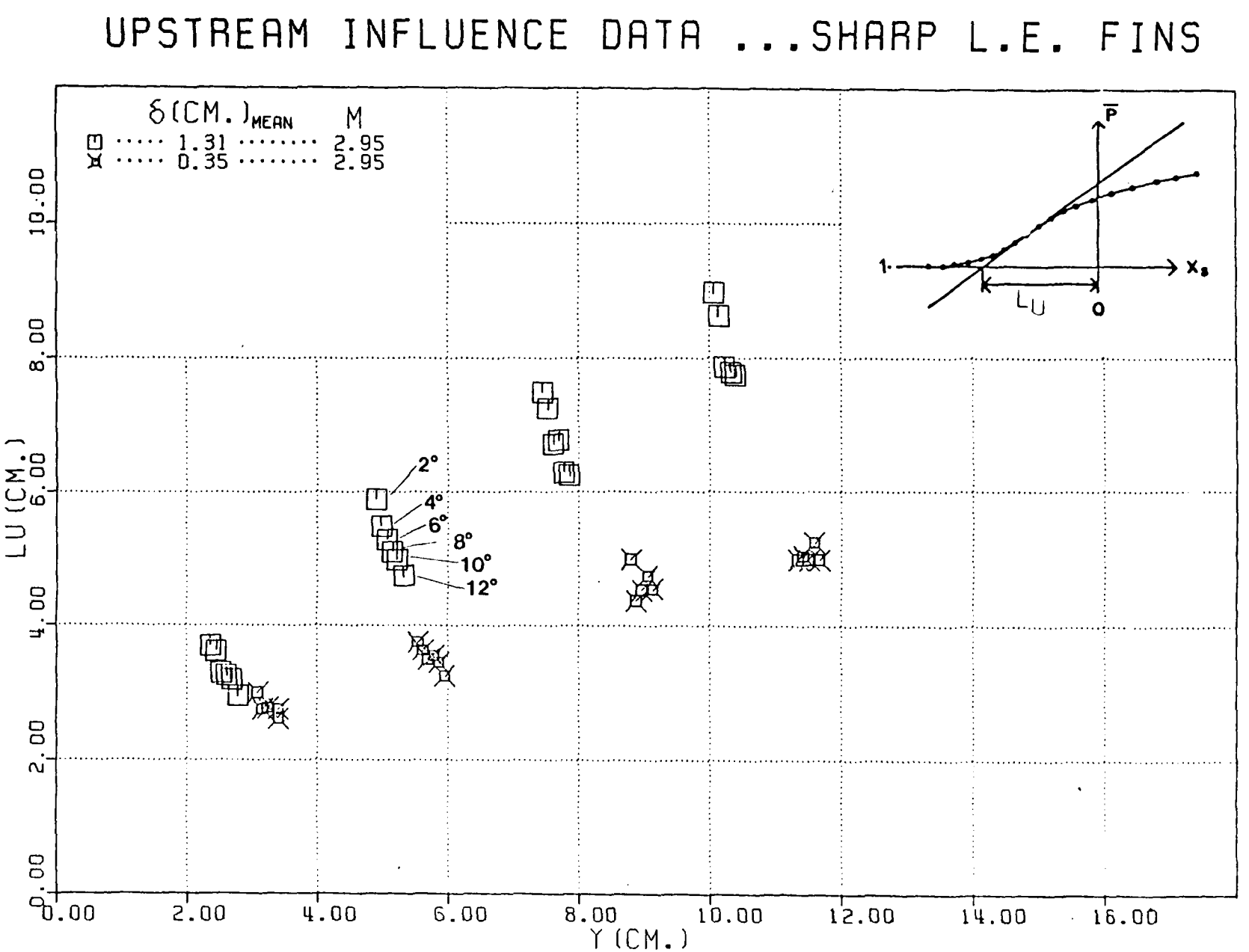

FIG. 5. Sharp Fin Upstream Influence versus Y

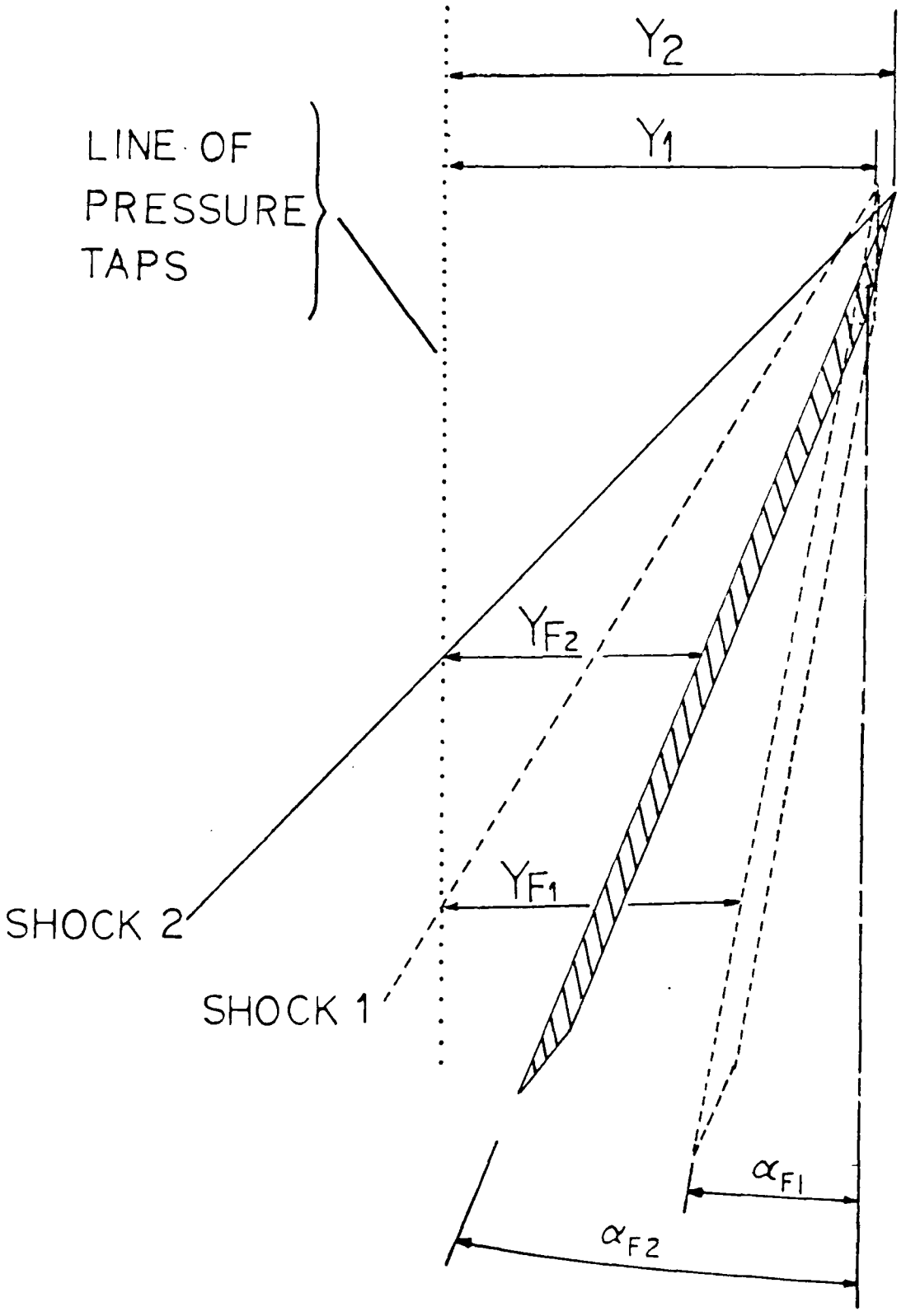

FIG. 6. Effect of Angle of Attack on Sharp Fin/Shock Wave Geometry

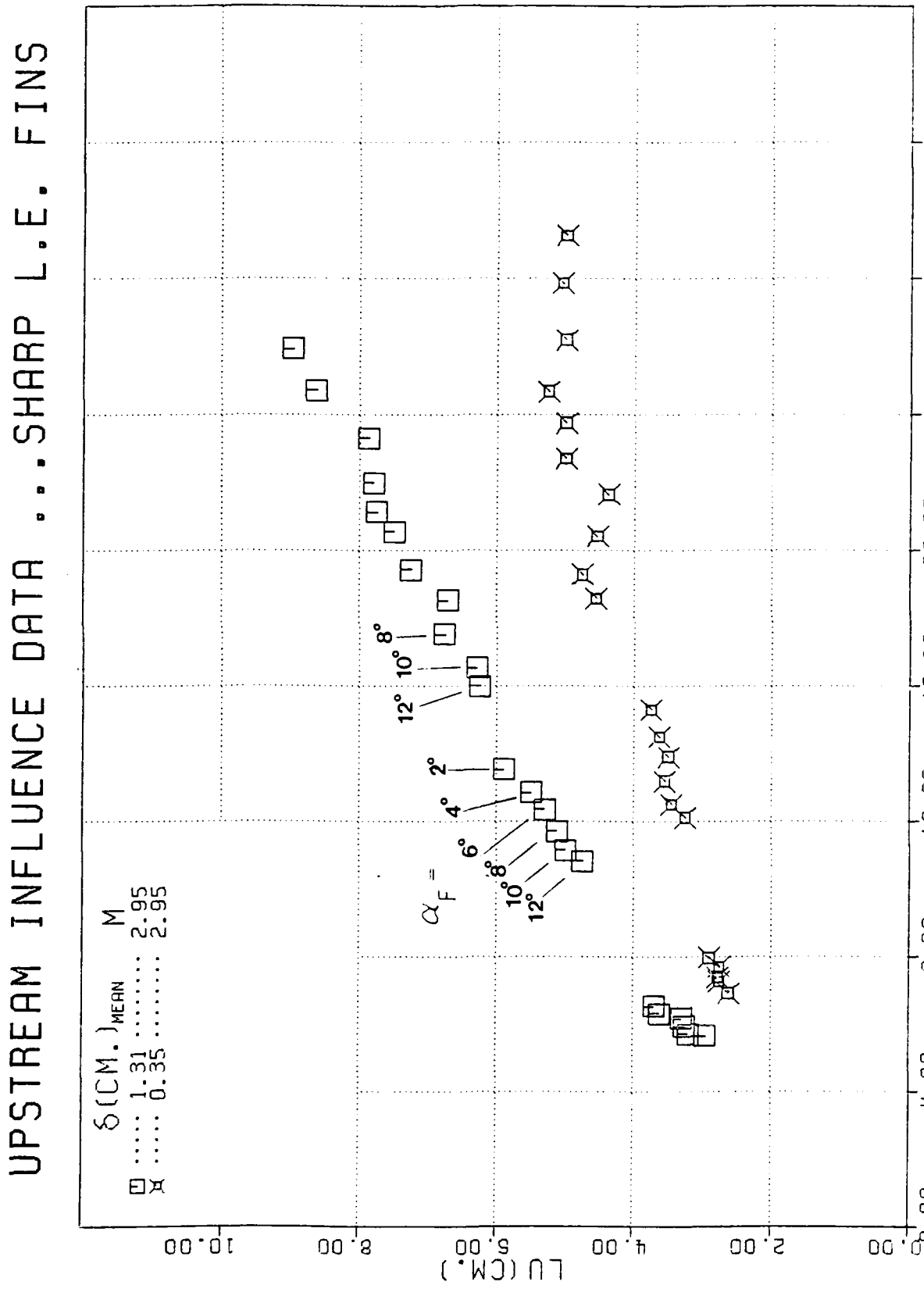

FIG. 7a. Sharp Fin Upstream Influence versus LSH

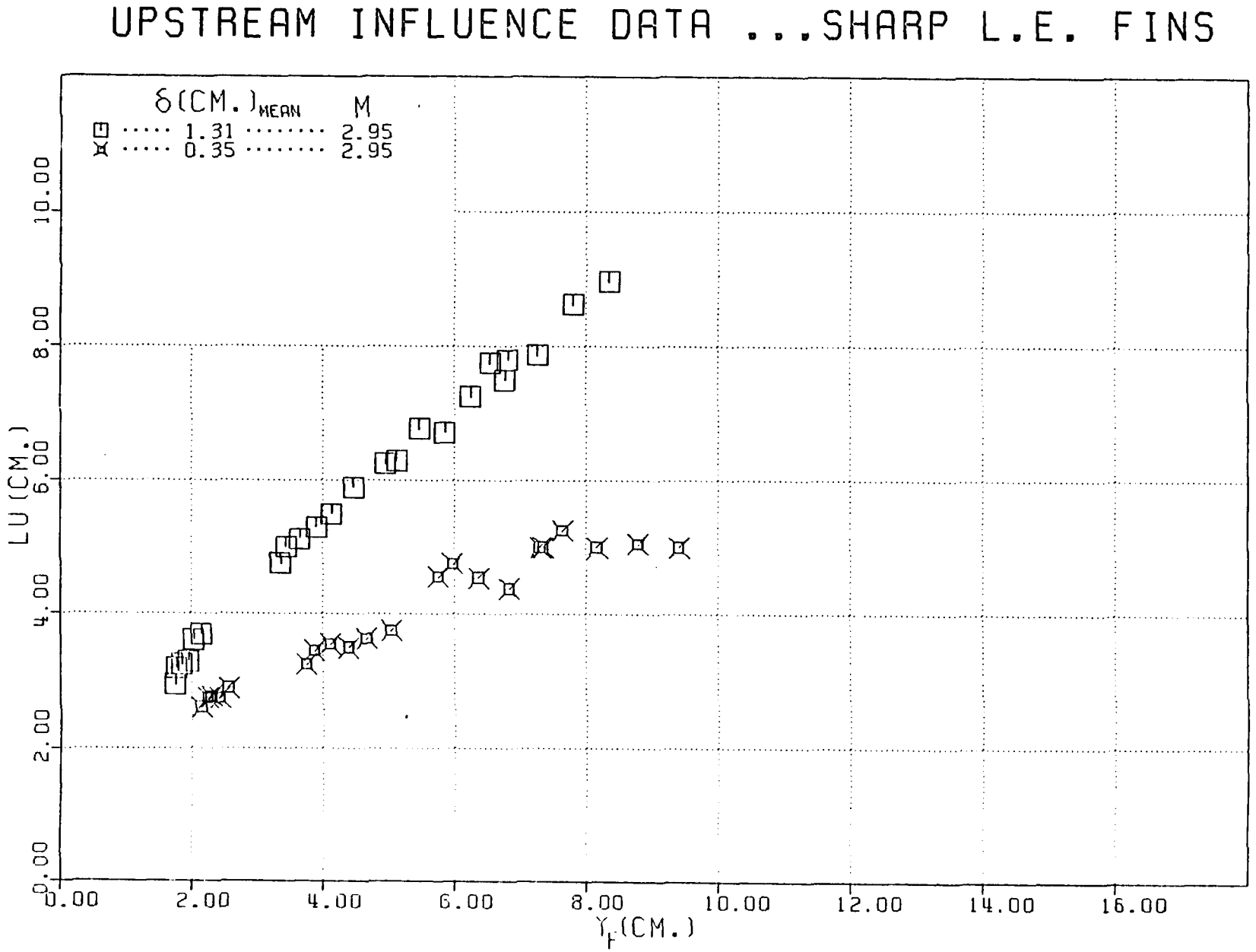

FIG. 7b. Sharp Fin Upstream Influence versus Y_F

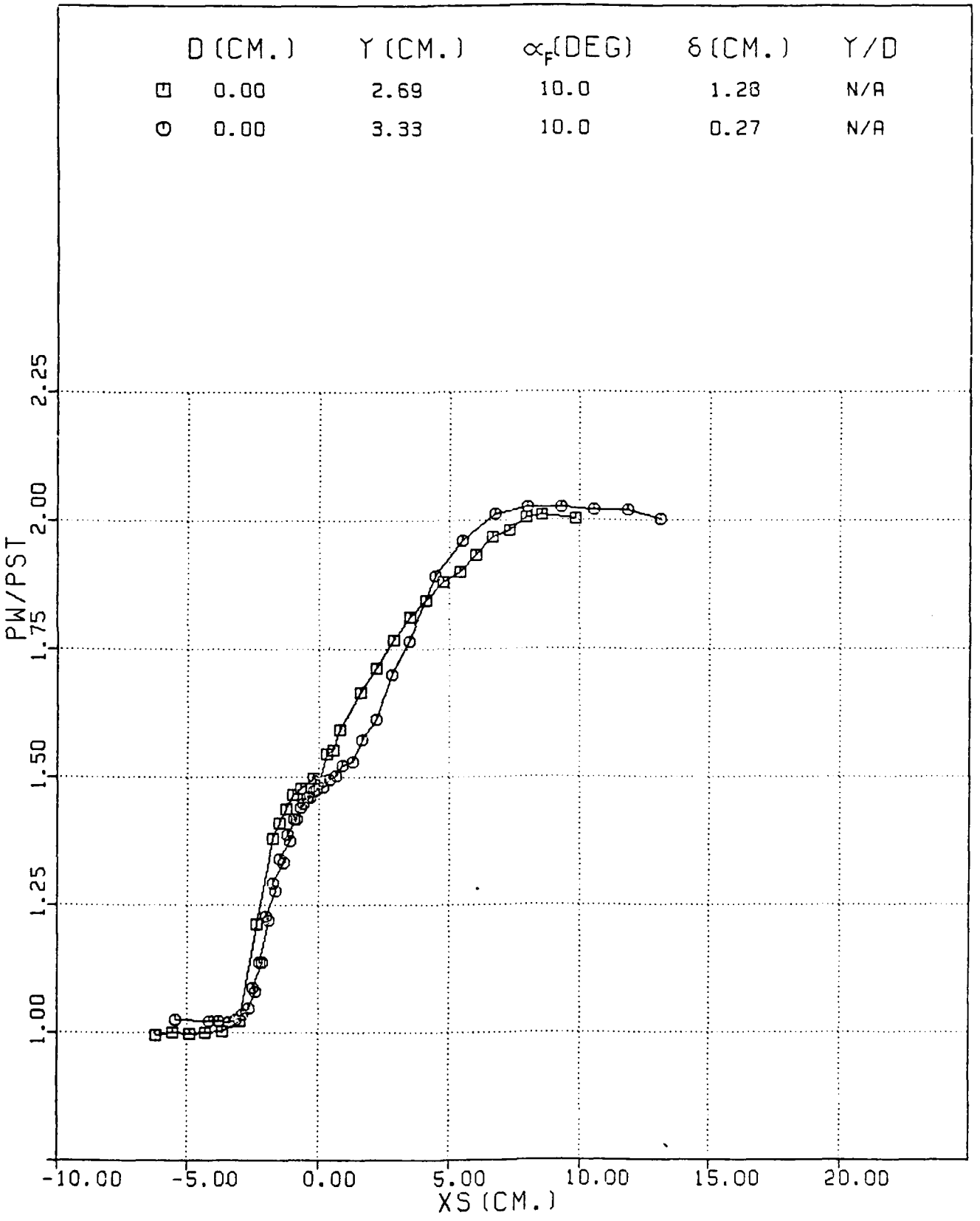

FIG. 8. Streamwise Pressure Distributions in Region Close to Sharp Fin

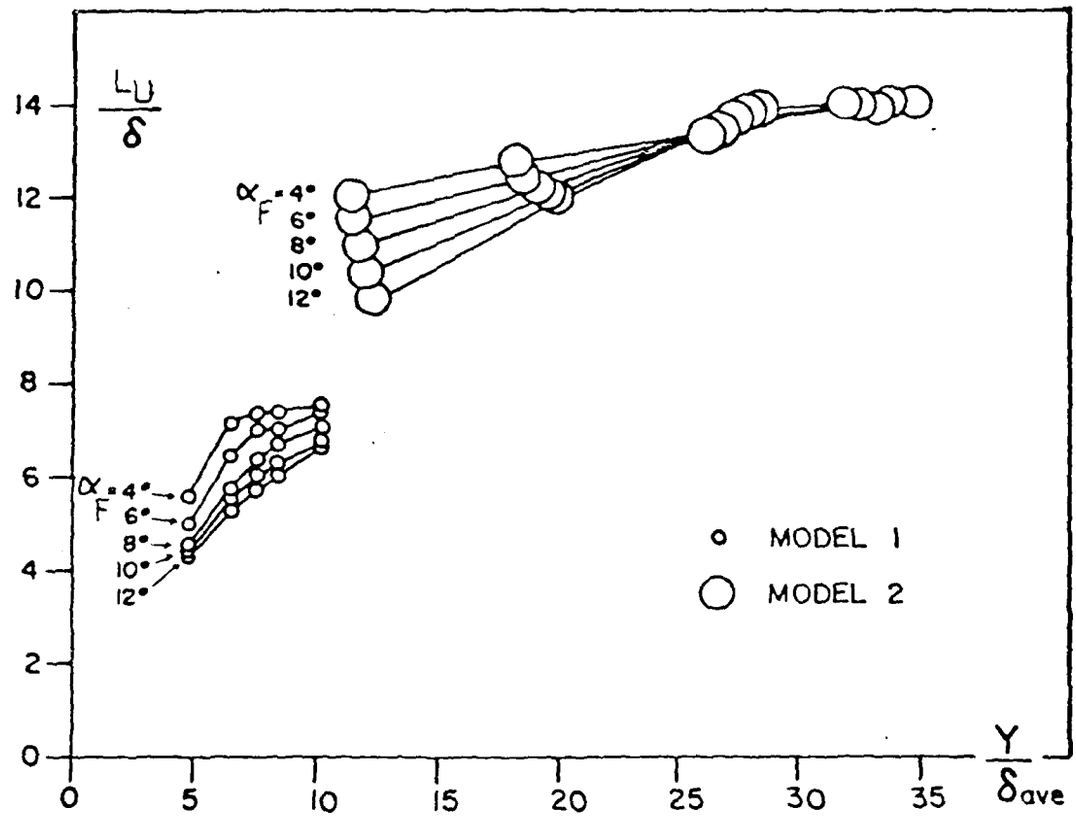

FIG. 9. Oskam's Correlation of Sharp Fin Upstream Influence Measurements

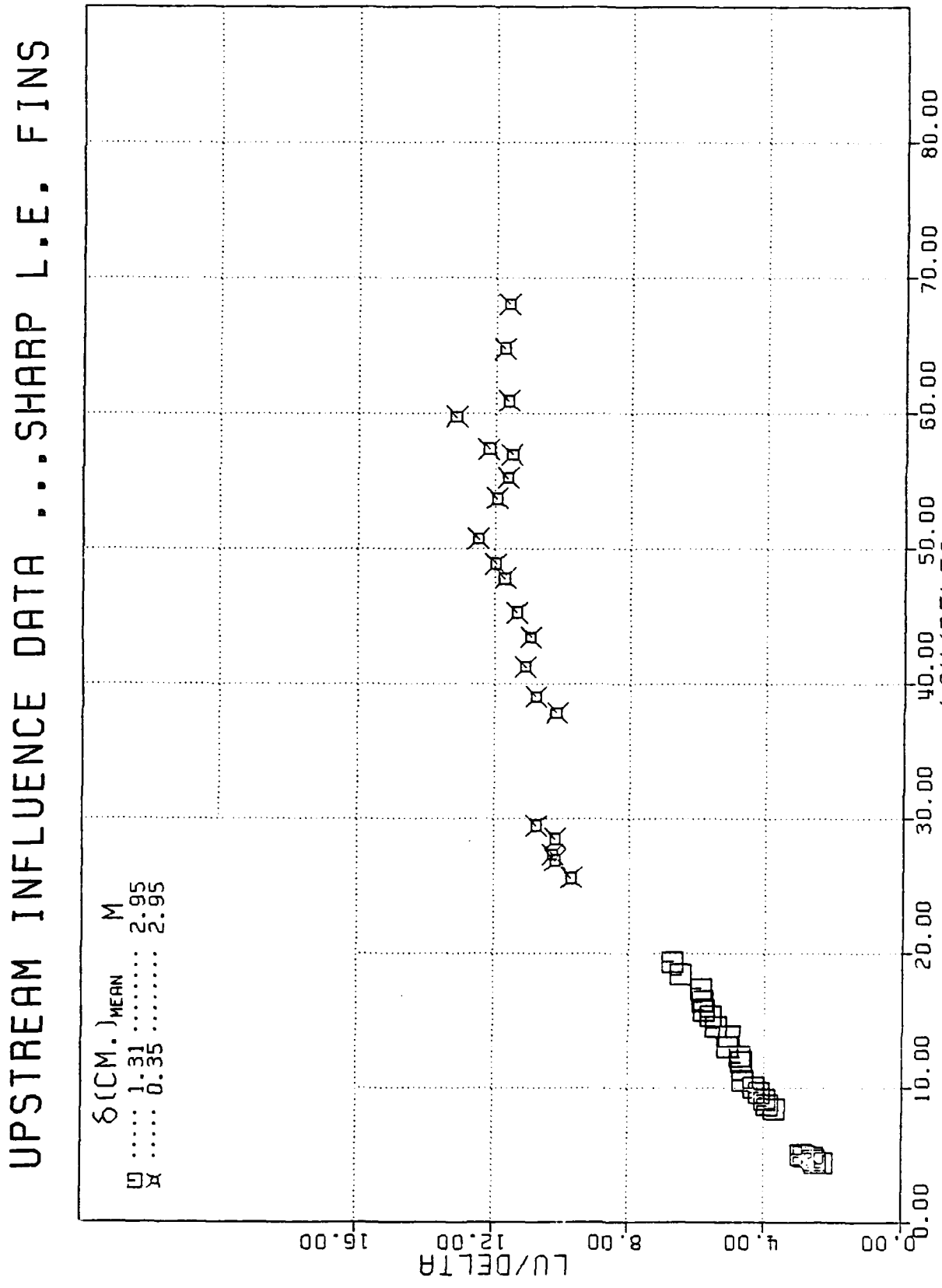

FIG. 10. Sharp Fin Upstream Influence Data in the Form L_u/δ versus LSH/δ

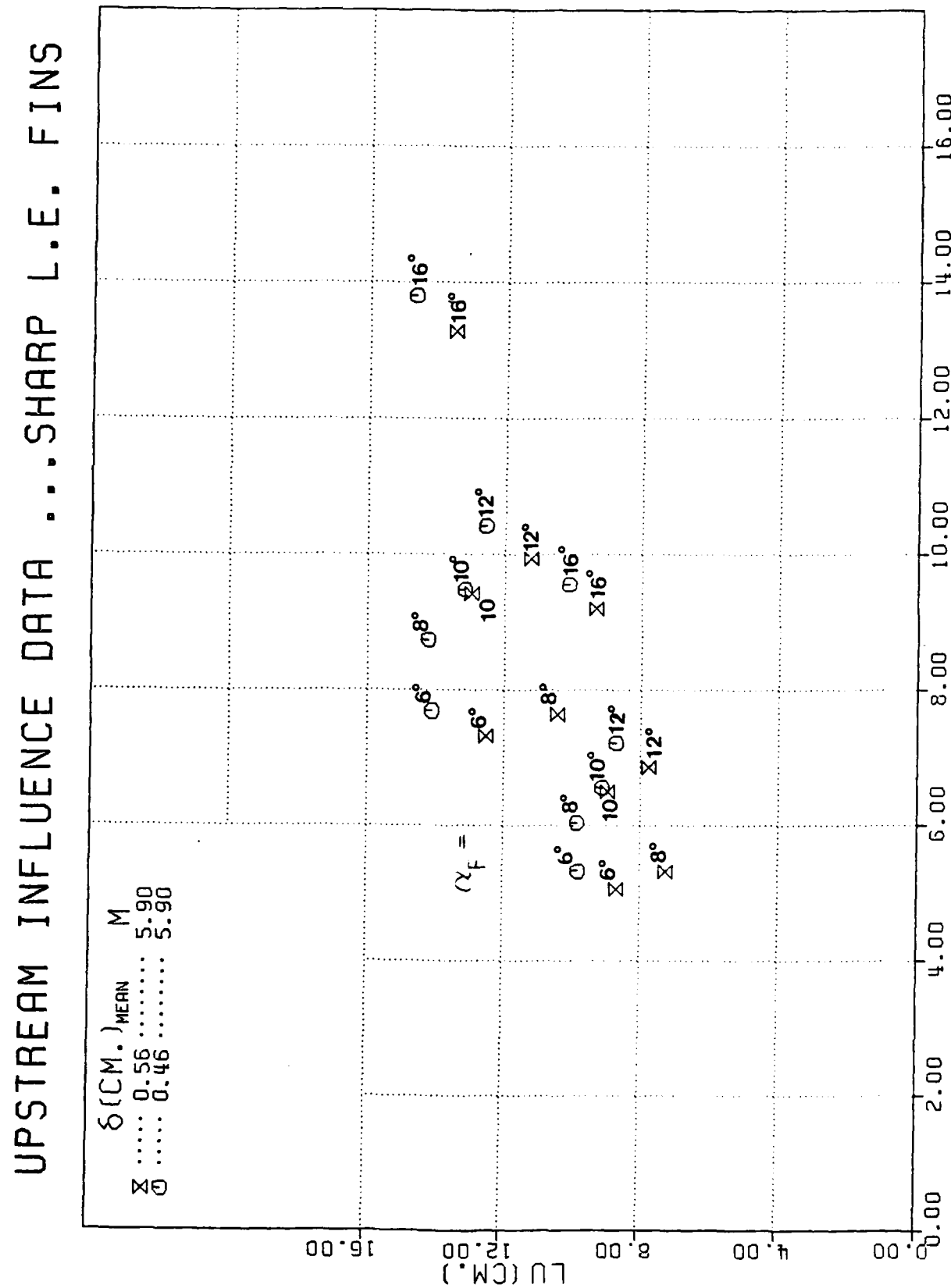

FIG. 11. Law's Sharp Fin Upstream Influence Measurements Plotted versus Y

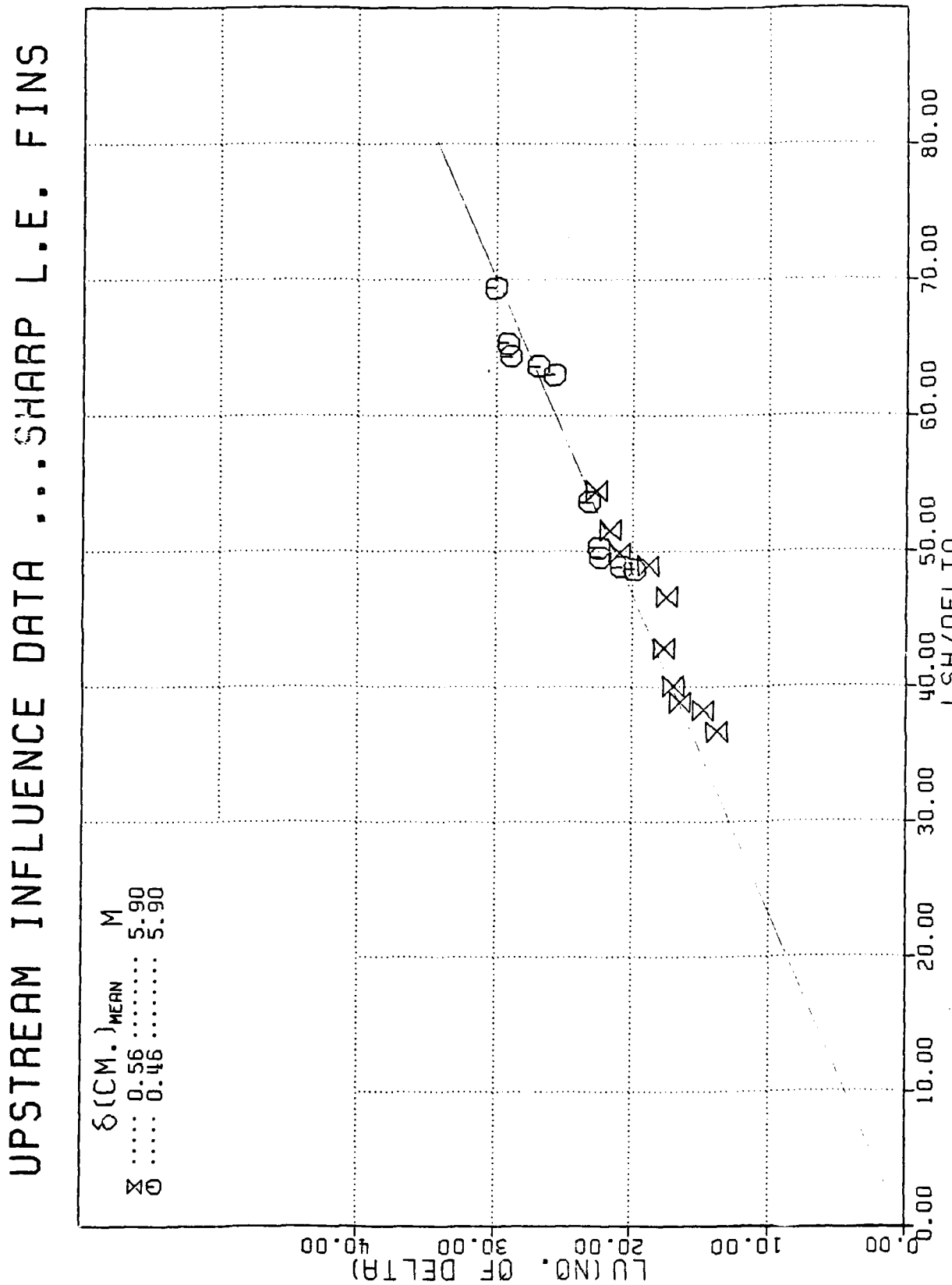

FIG. 12. Law's Sharp Fin Upstream Influence Measurements in the Form L_u/δ versus LSH/δ

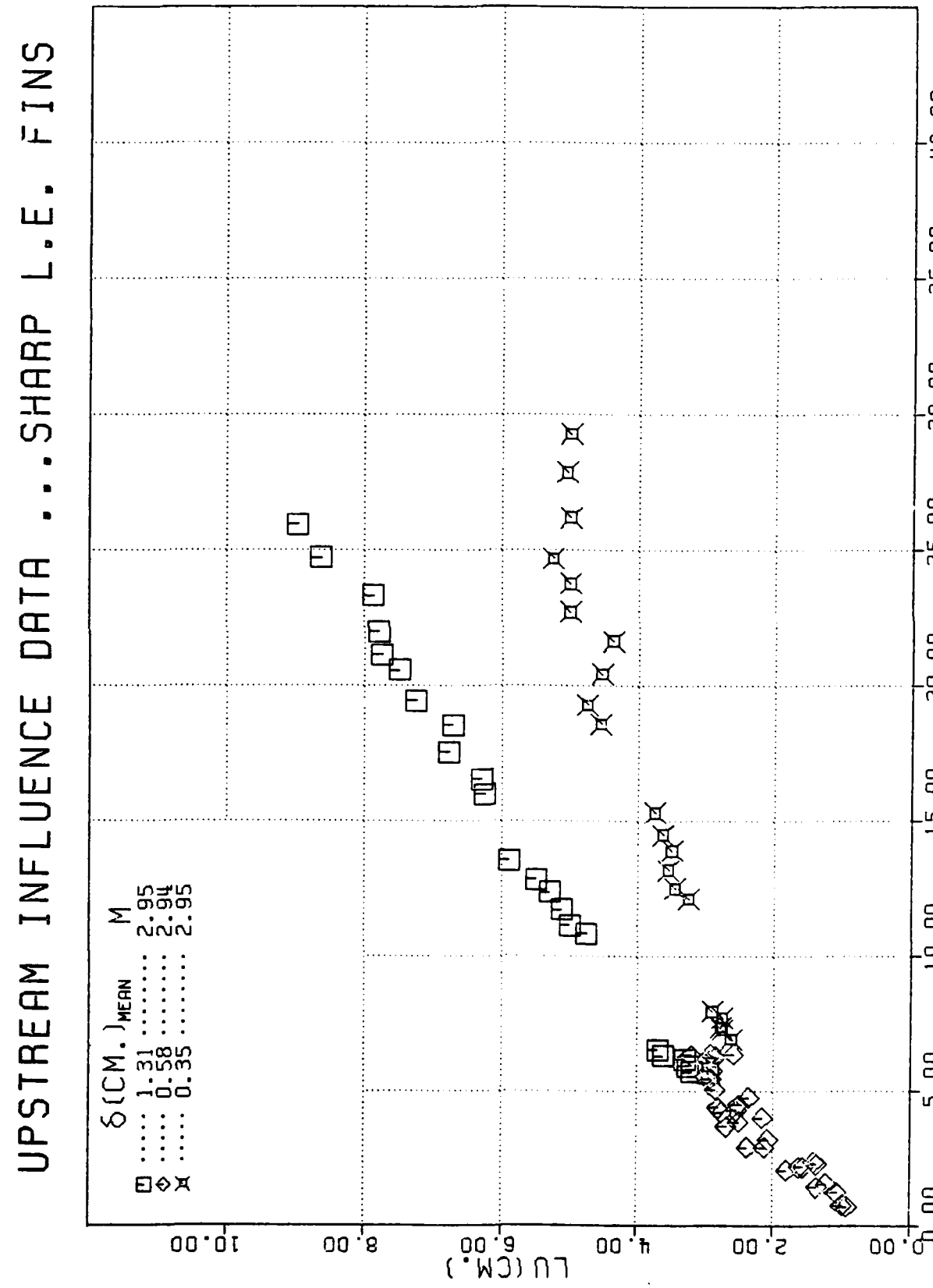

FIG. 13. Sharp Fin Upstream Influence Data of McCabe and Princeton University [L_u/δ vs. LSH]

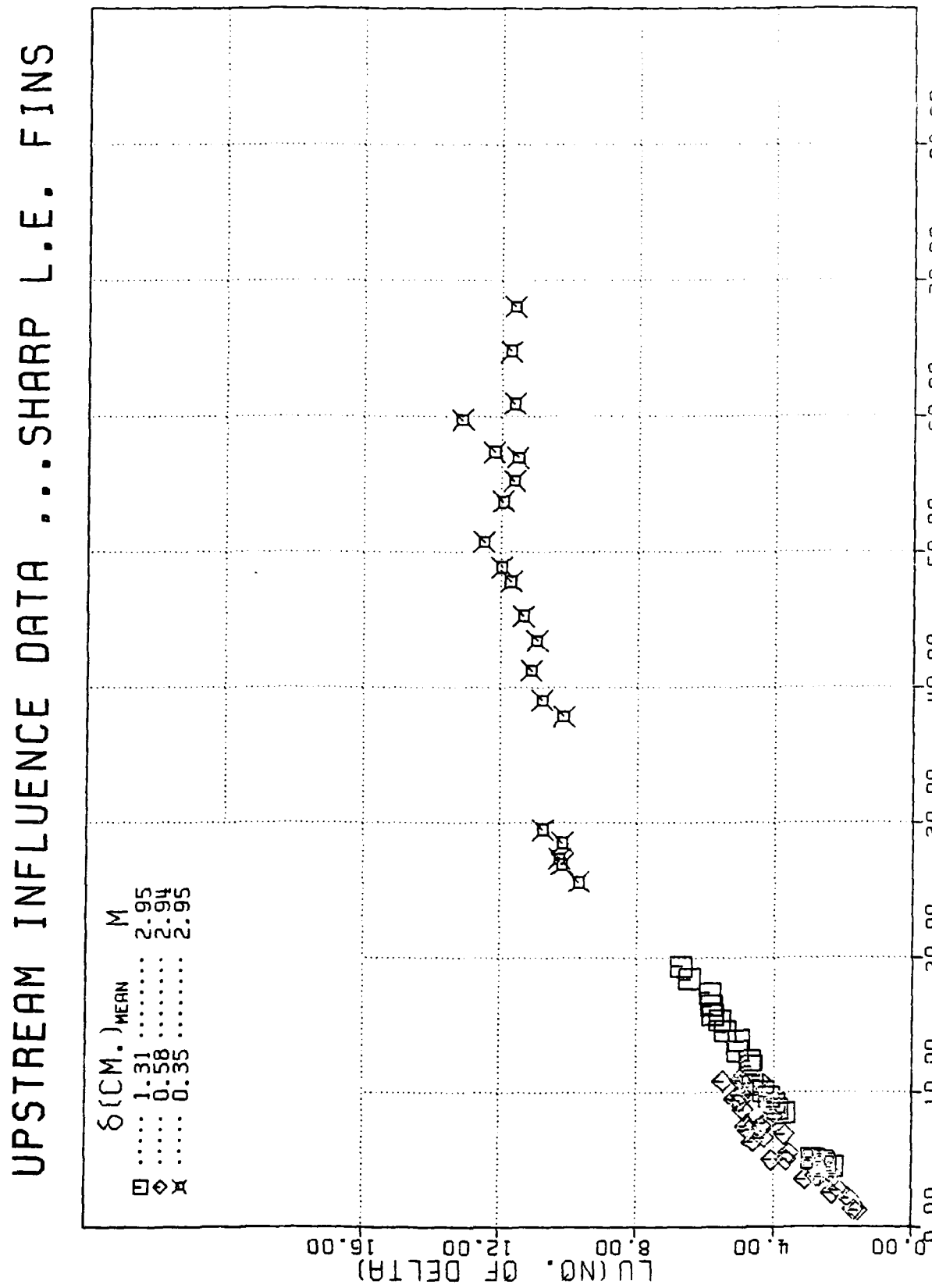

FIG. 14. Sharp Fin Upstream Influence Data of McCabe and Princeton University $[L_u/\delta$ vs. LSH/$\delta]$

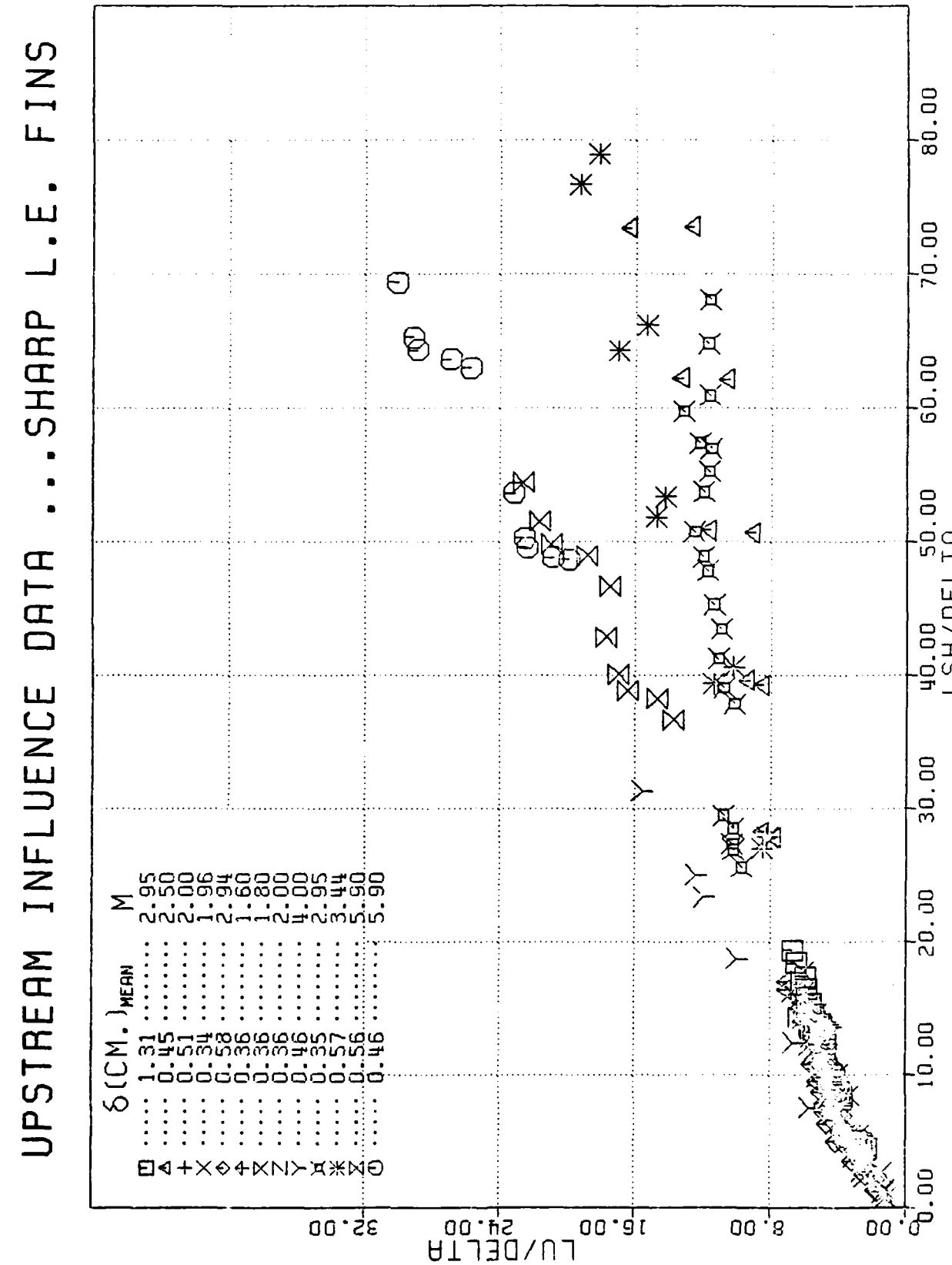

FIG. 15. Effect of Mach Number on Sharp Fin Upstream Influence

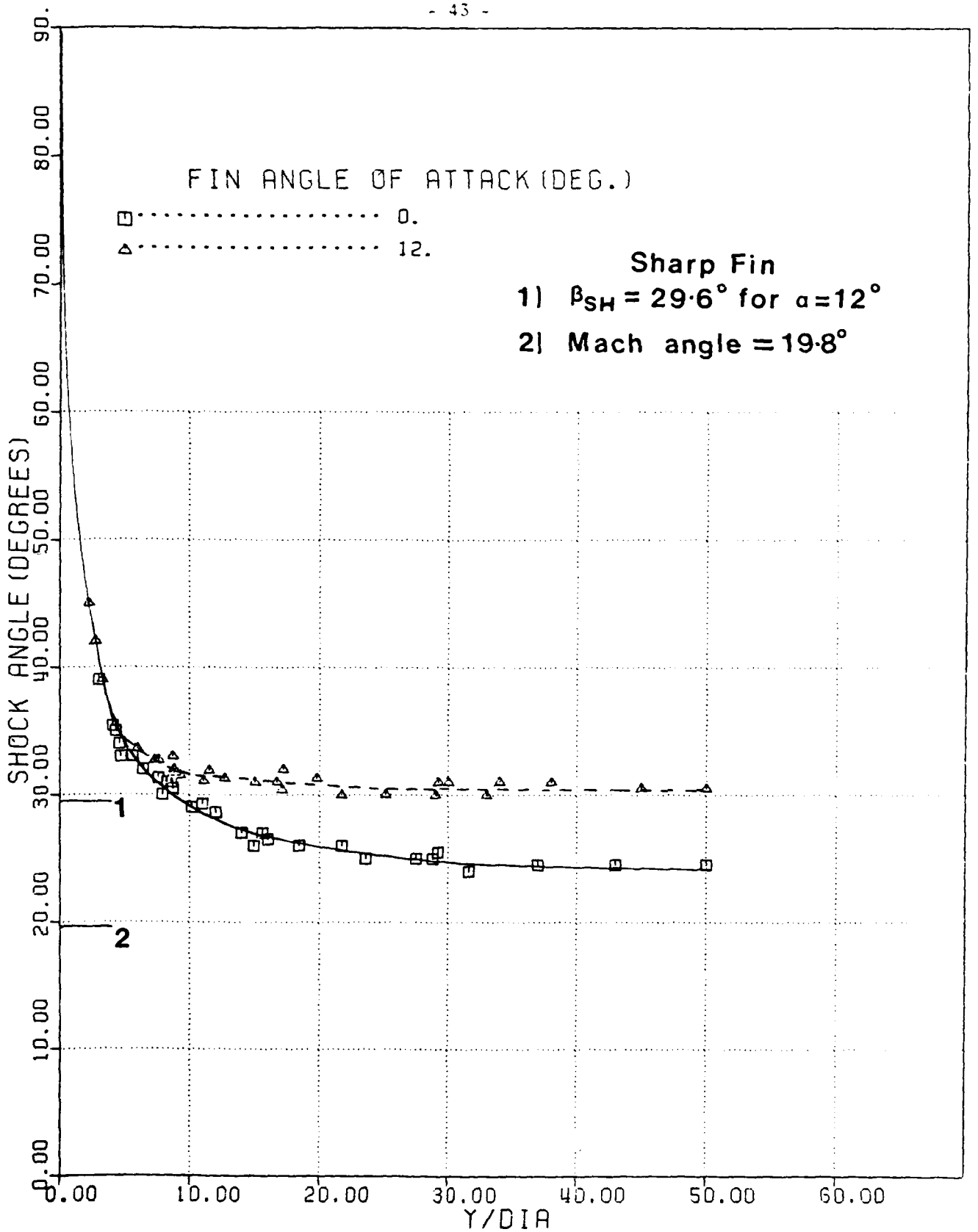

FIG. 16. Blunt Fin-Induced Shock Wave Angle as a Function of Y/D

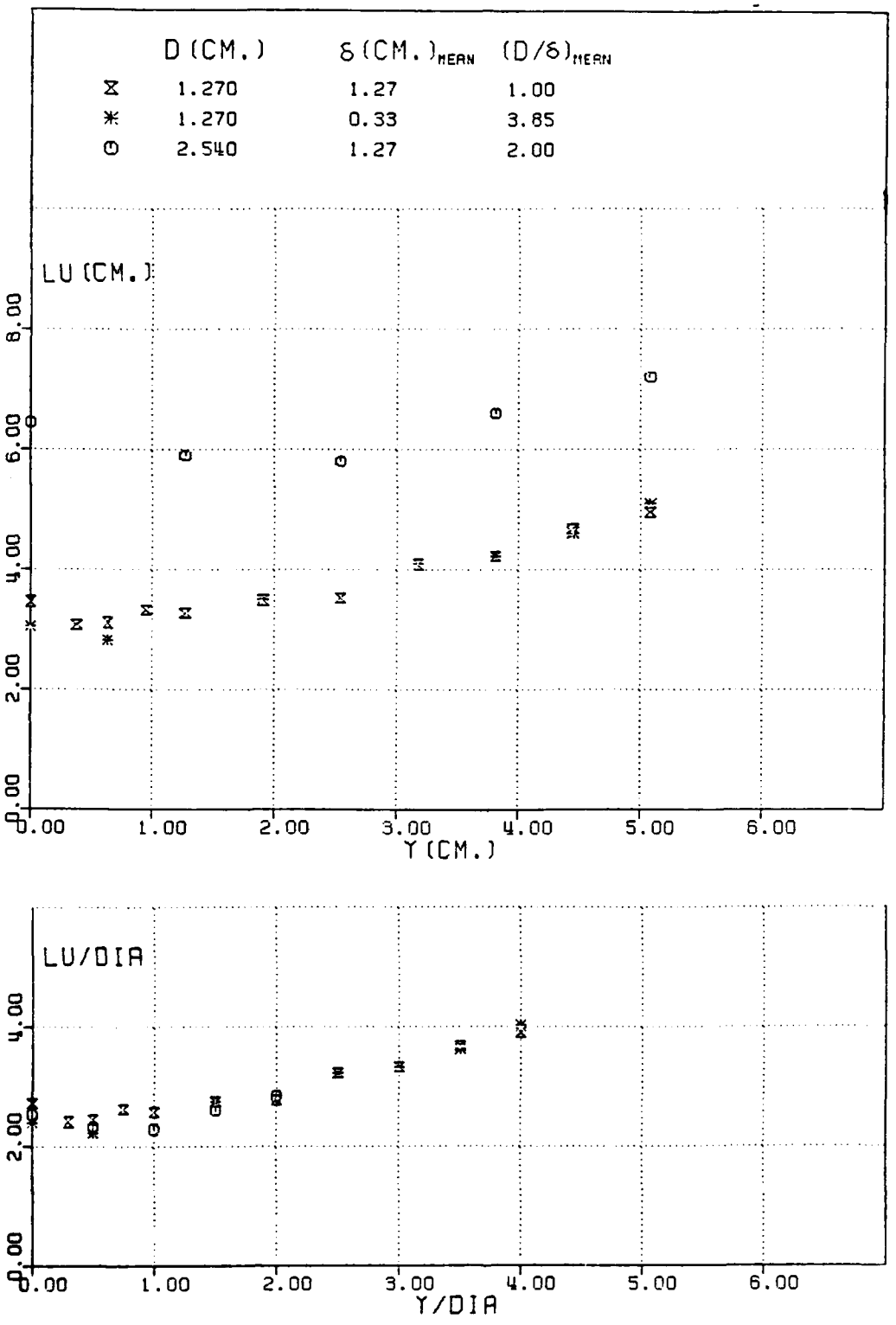

FIG. 17. Blunt Fin Upstream Influence Data in Range $0 \leq Y/D \leq 4$

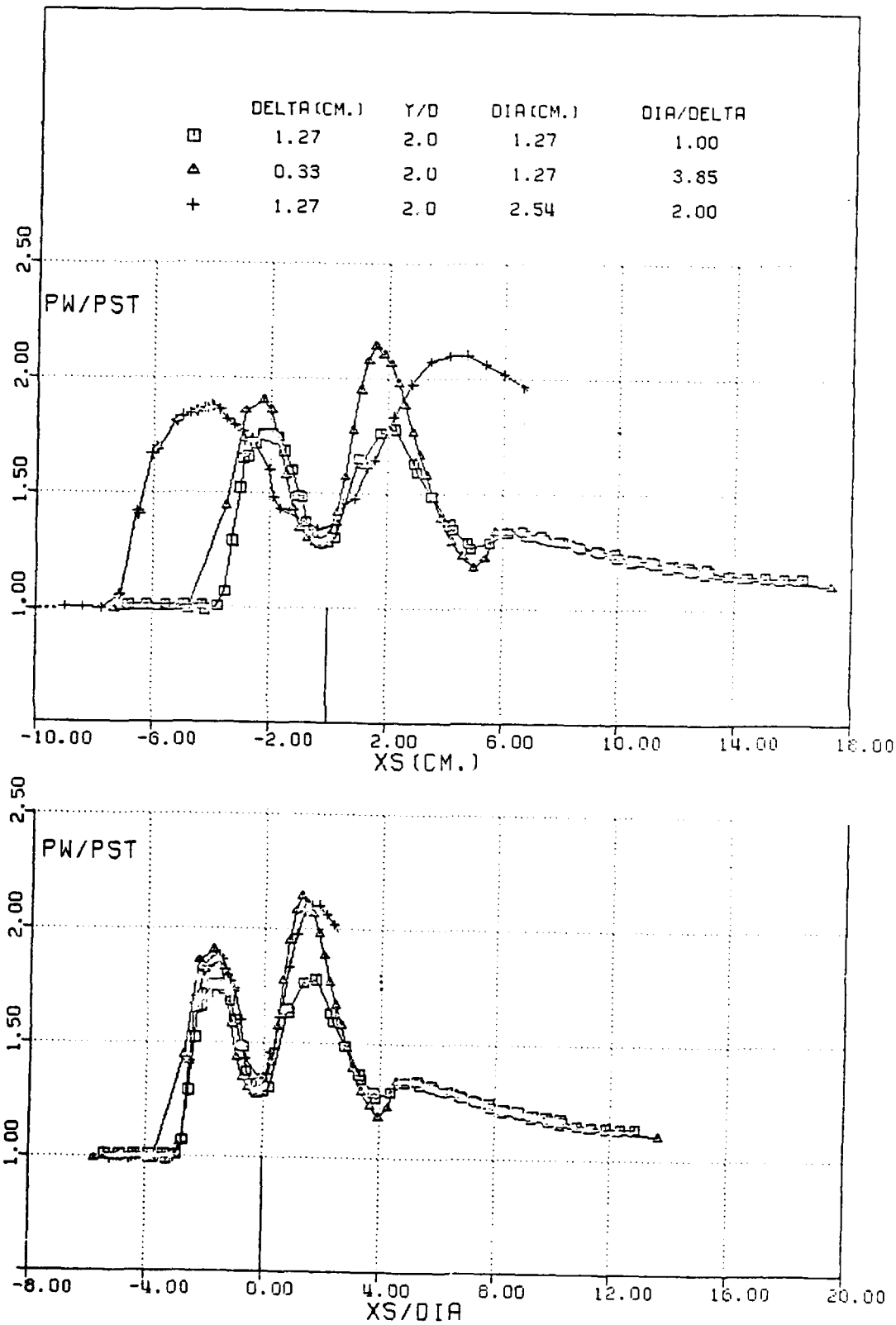

FIG. 18. Streamwise Pressure Distributions at Y/D = 2

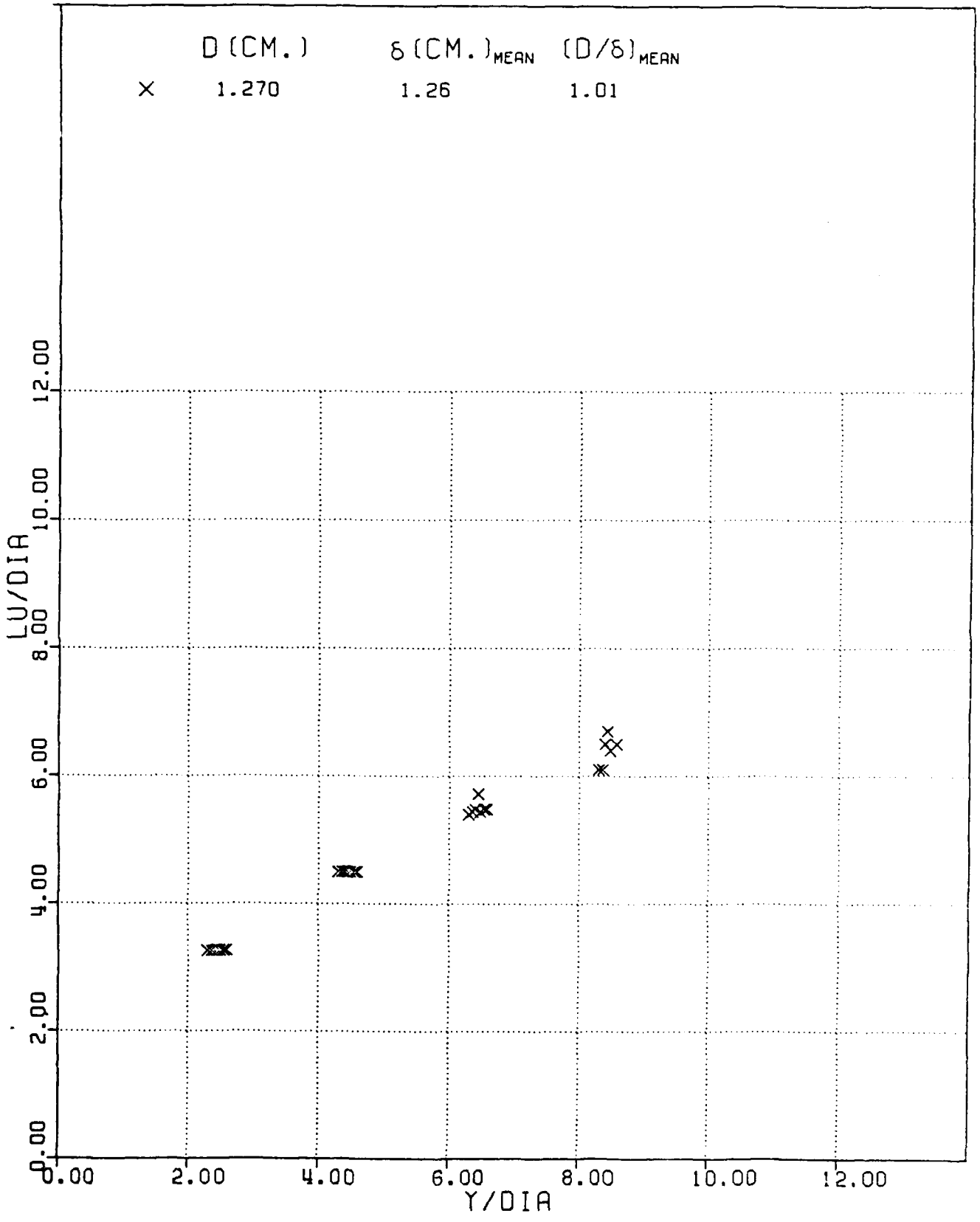

FIG. 19. Effect of Angle of Attack on Blunt Fin (D = 1.27cm) Upstream Influence

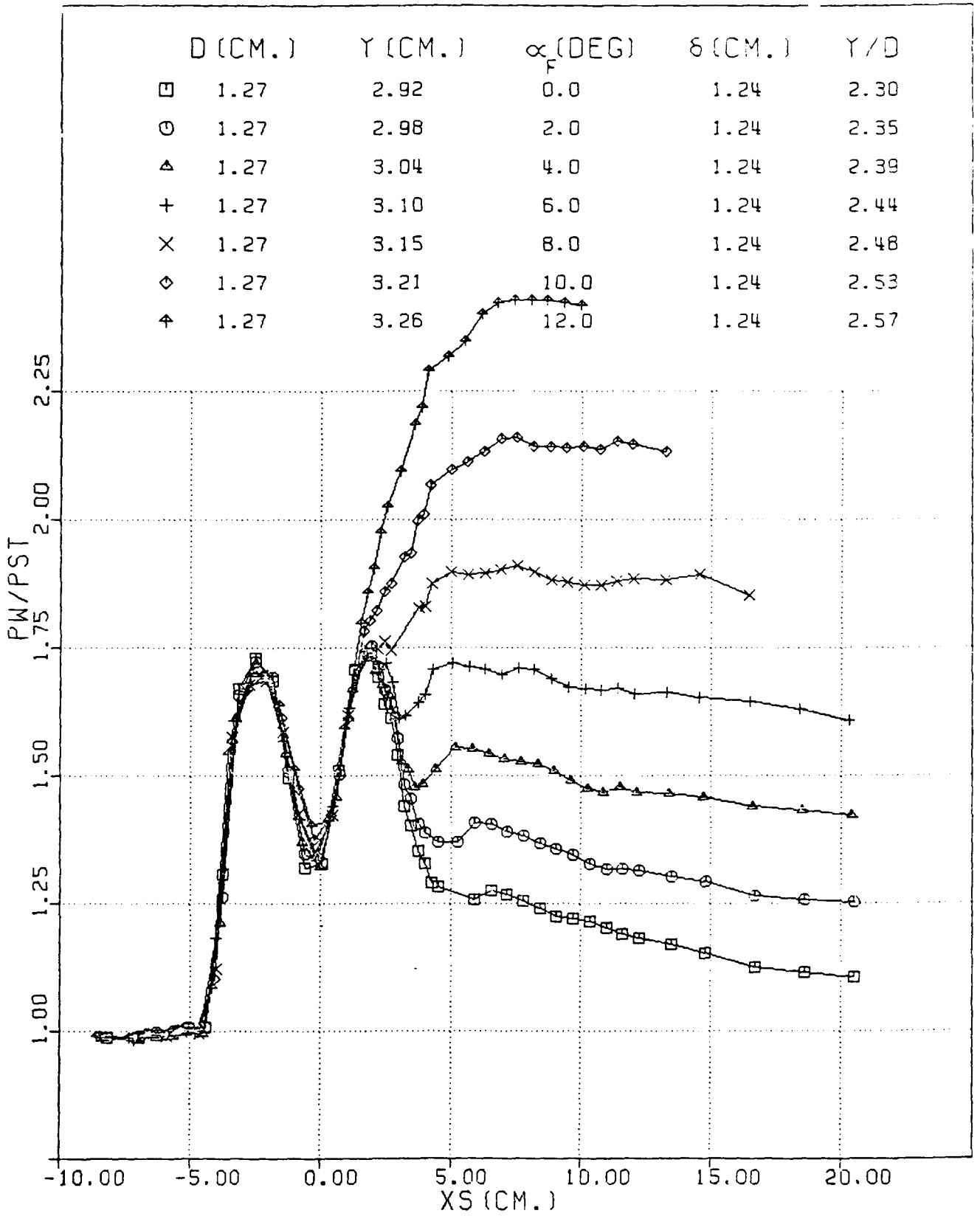

FIG. 20. Effect of Angle of Attack on Blunt Fin (D = 1.27cm) Streamwise Pressure Distribution

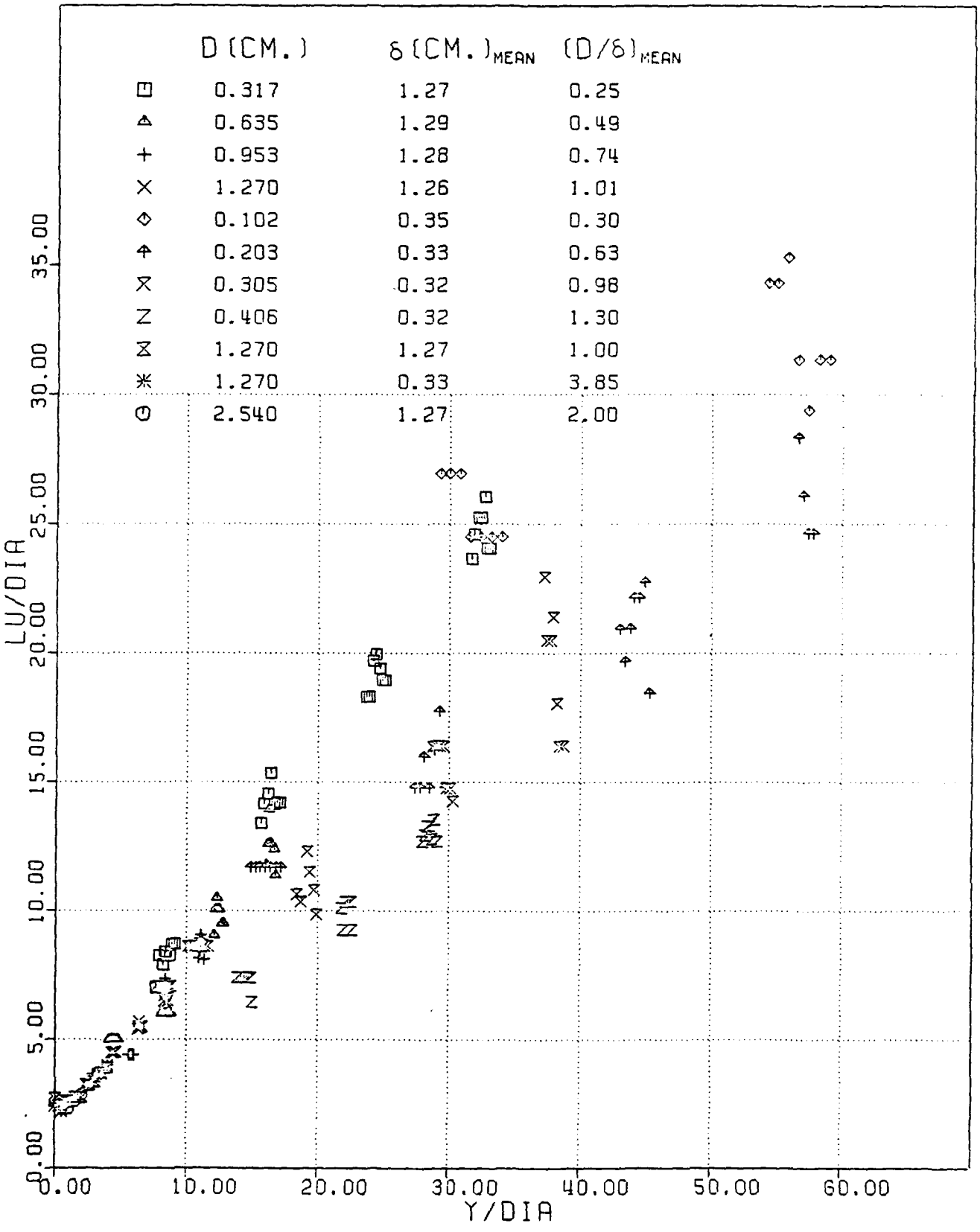

FIG. 21. Upstream Influence Data From all Blunt Fins Tested in Model 1 and 2 Studies

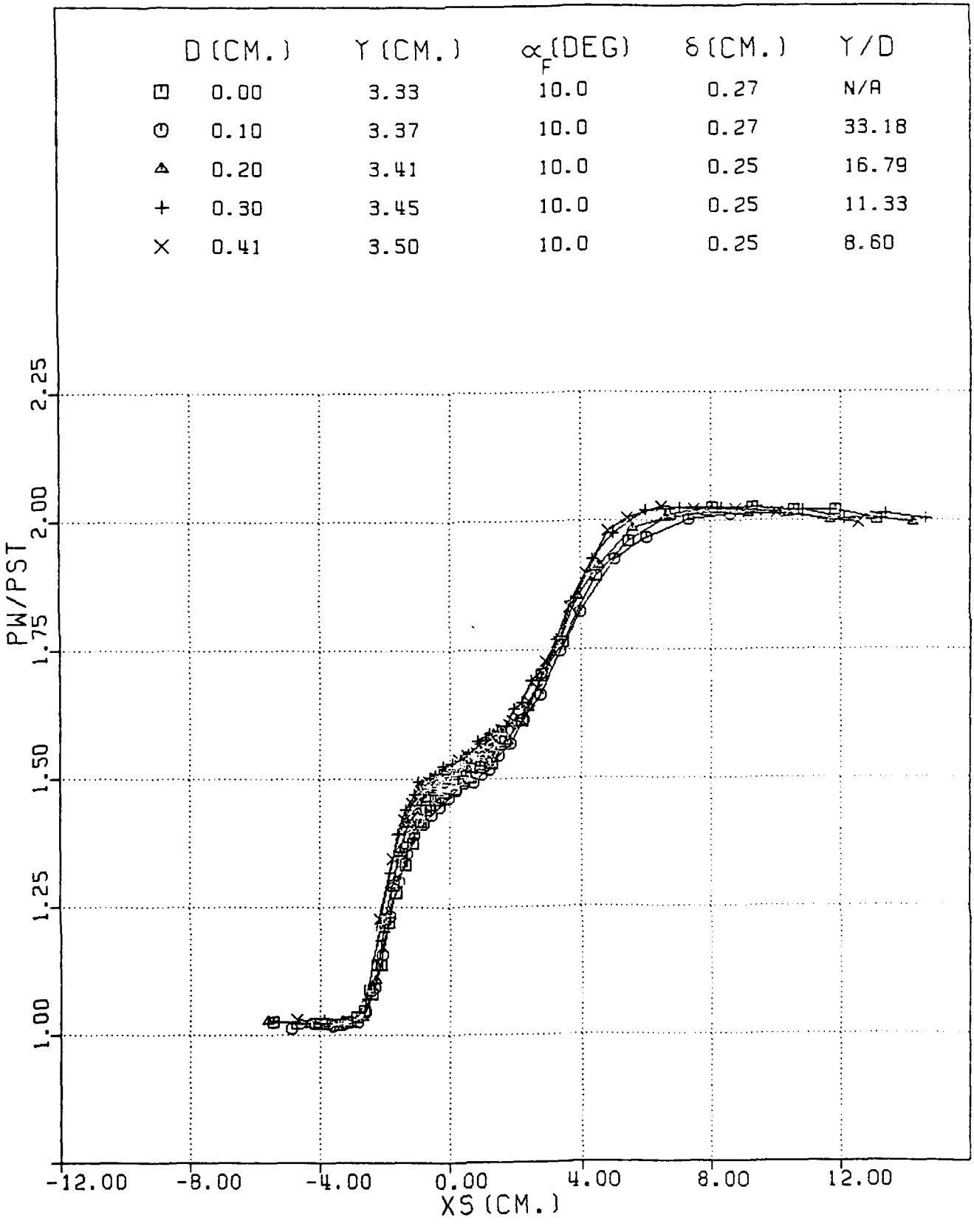

FIG. 22. Comparison of Model 2 Blunt and Sharp Fin Streamwise Pressure Distributions in Range Y/D > 8.6 at $\alpha_F = 10°$

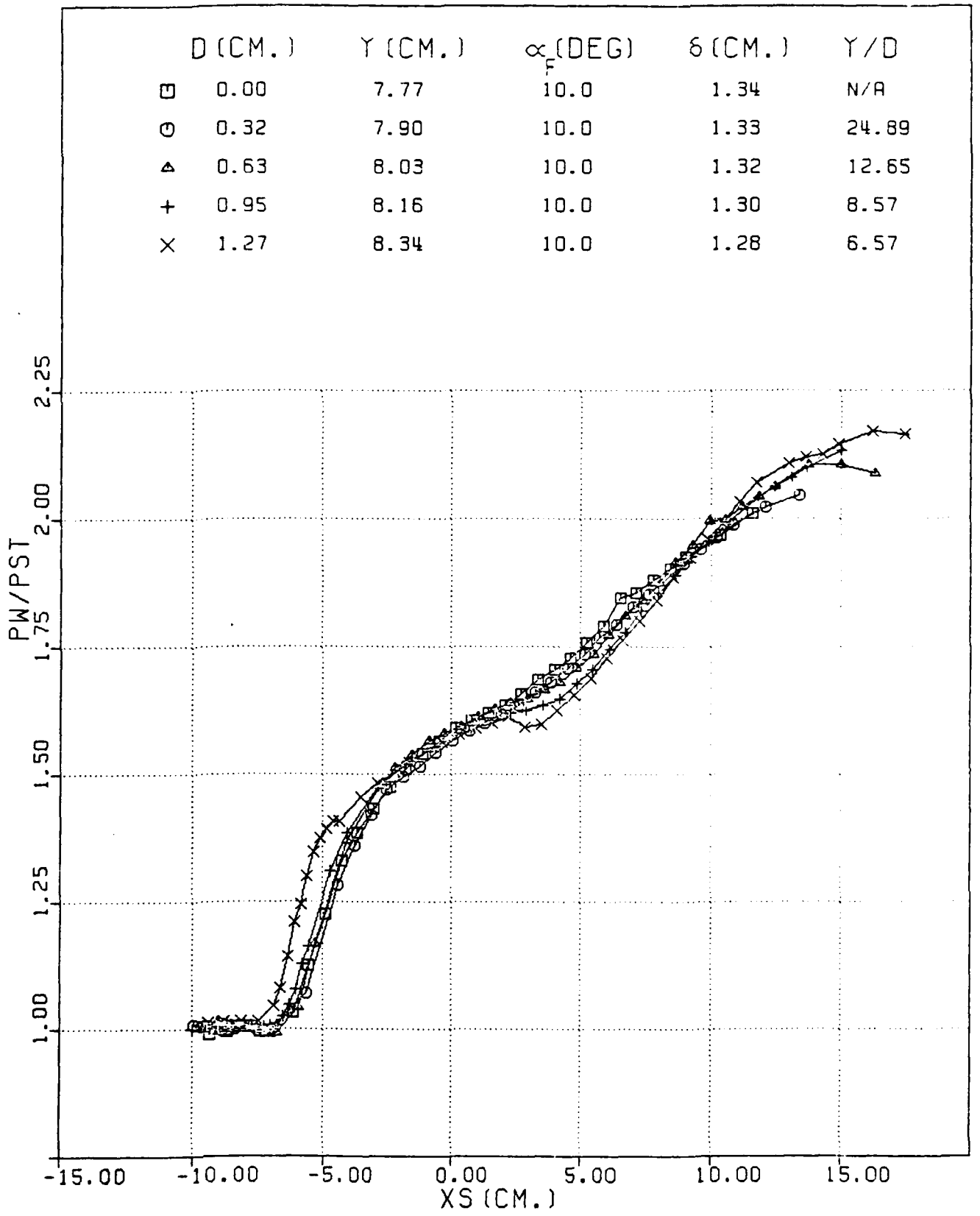

FIG. 23. Comparison of Model 1 Blunt and Sharp Fin Streamwise Pressure Distributions in Range Y/D > 6.6 at $\alpha_F = 10°$

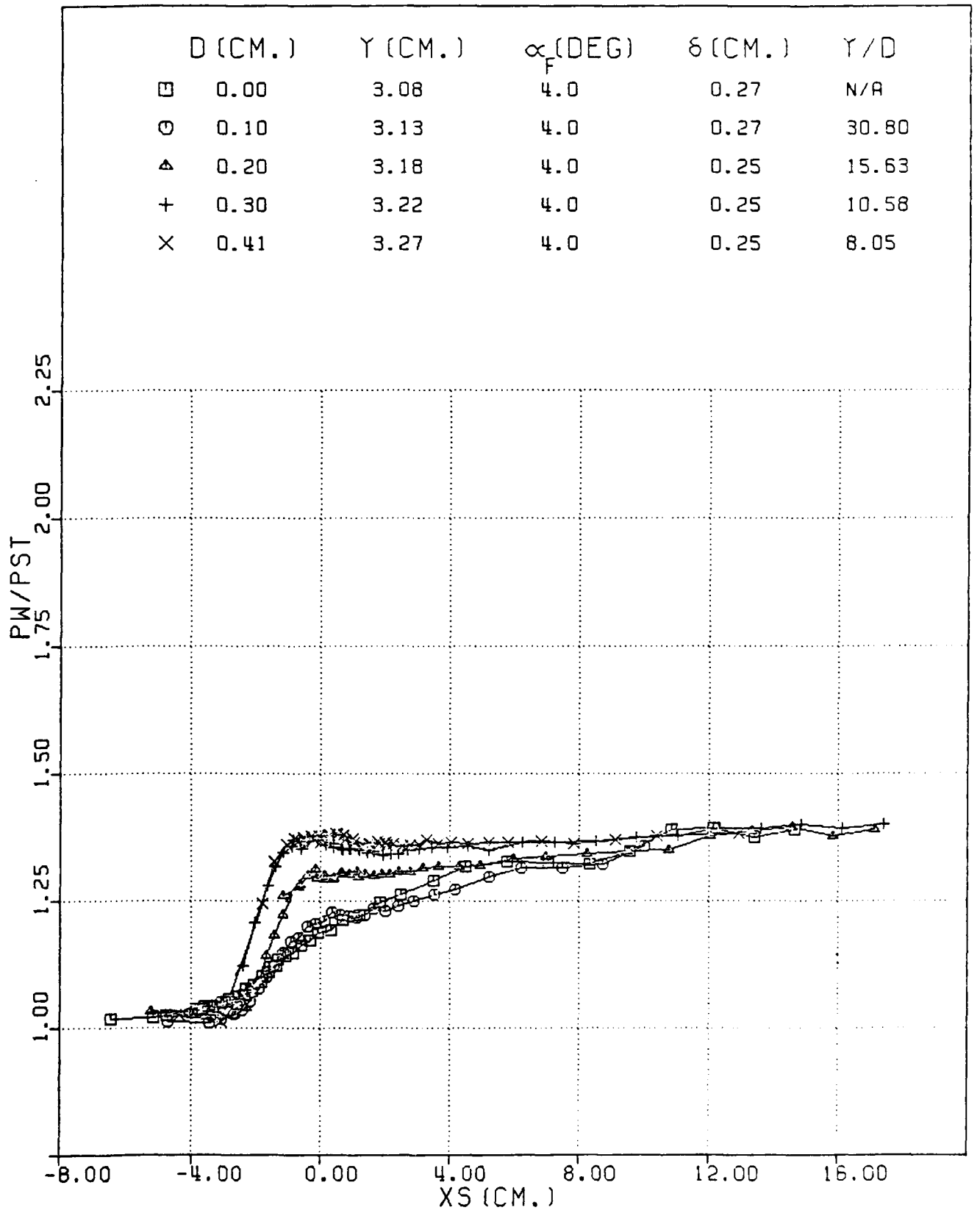

FIG. 24. Comparison of Model 2 Blunt and Sharp Fin Streamwise Pressure Distributions in Range Y/D > 8.0 at α_F = 4°

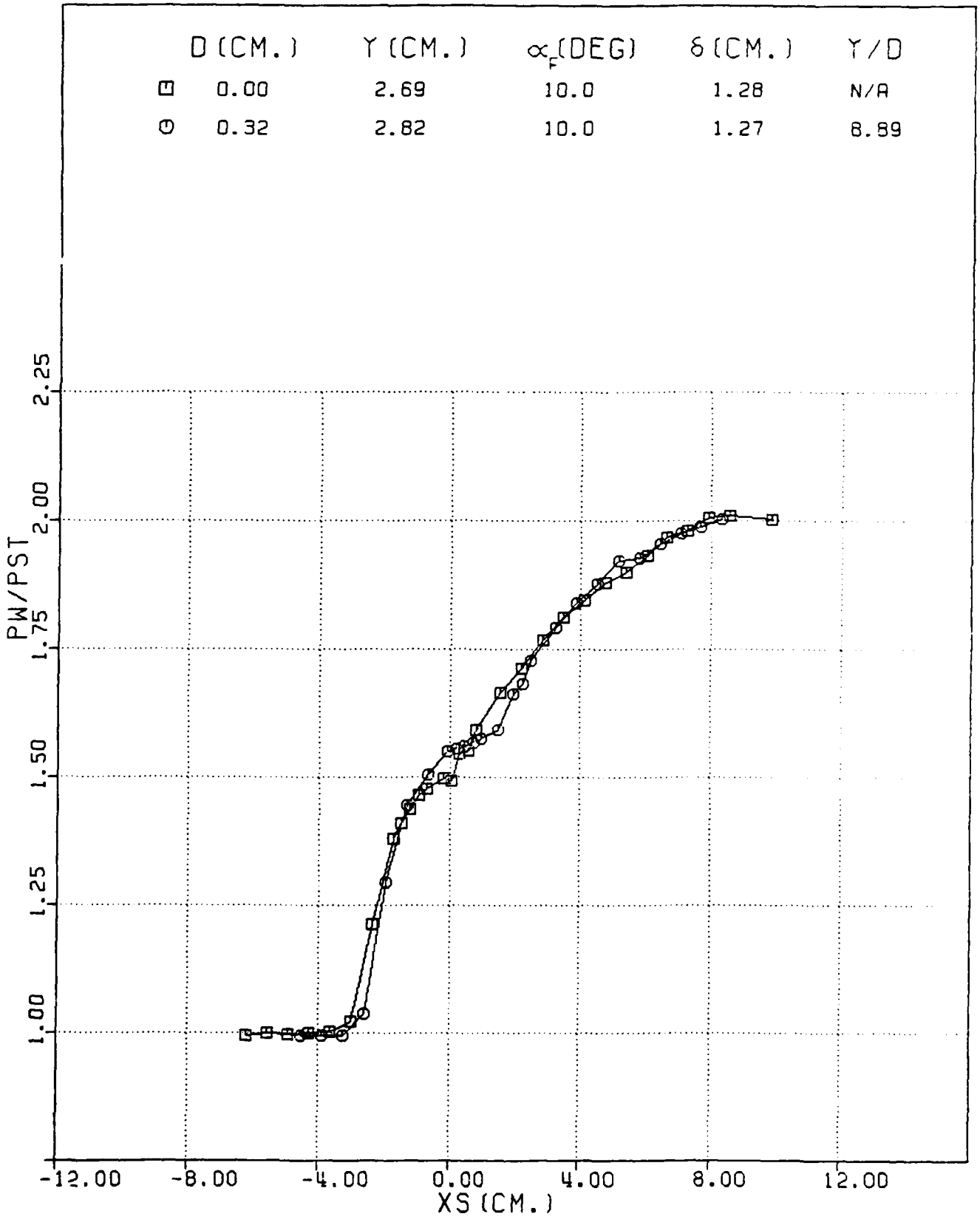

FIG. 25. Model 1 Streamwise Pressure Distributions Outside of Nose-Dominated Region

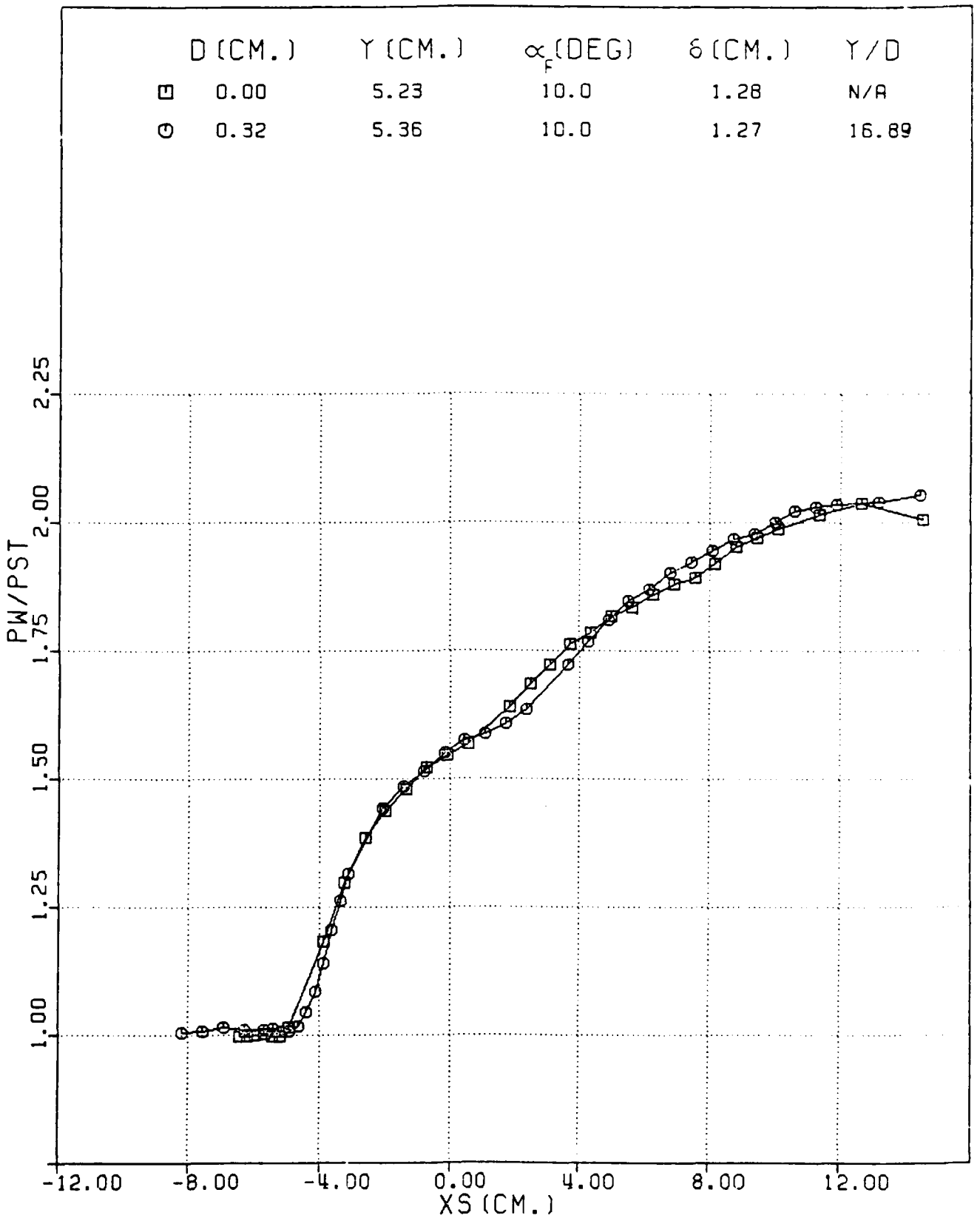

FIG. 26. Model : Streamwise Pressure Distributions Outside of Nose-Dominated Region

END

DATE
FILMED

8-80

DTIC